Alvarado, G. E., Schmincke, H.-U. and Campos-Durán, D. (2026) “Intra-crater clast recycling and flow confinement during the moderate 1963–1965 eruption at Irazú volcano (Costa Rica)”, *Volcanica*, 9(1). doi: 10.30909/vol/oazi2503.

RESEARCH ARTICLE

VOLCANICA

Intra-crater clast recycling and flow confinement during the moderate 1963–1965 eruption at Irazú volcano (Costa Rica)

Guillermo E. Alvarado [α], Hans-Ulrich Schmincke[β], and Daniela Campos-Durán [*γ]

[α] Centro en Investigación de Ciencias Geológicas, Universidad de Costa Rica, San José, Costa Rica.

[β] Geomar, Wischhofstrass. 1-4, Kiel, D-24148 Kiel, Germany.[†]

[α] Escuela de Ciencias Geográficas, Universidad Nacional, Heredia, Costa Rica.

Submitted: 2024-09-24 | In Review: 2026-04-13 | Published: 2026-06-12

Editor: A. Hornby | Production: B. Hosseini, J. Farquharson

Abstract

Despite extensive contemporary documentation of the 1963–1965 Irazú eruption, a detailed analysis of its proximal tephra deposits has been lacking. Here, we characterize the stratigraphy and sedimentology of these deposits, interpret their depositional processes including tephra recycling, and constrain magma recharge timing through geochemical data. The eruption was predominantly phreatomagmatic, with subordinate Strombolian and rare phreatic events, producing ~6.2×10^7 m^3 of tephra (DRE: 5.68×10^7 m^3; VEI 3). Four eruptive stages were identified by correlating deposits with contemporary observations. The irregular pre-1963 crater morphology controlled the development of an asymmetrical tuff cone and a maar-like crater. Intra-crater deposits (~28 m) and rim deposits (~5.7 m) include fallout beds, ballistic curtain deposits, dilute pyroclastic density currents, and massive ash beds. The steep, funnel-shaped crater promoted significant tephra fallback and recycling, and confinement of pyroclastic flow deposits. The deposits record compositional enrichment in incompatible elements from June 1964 indicating magma recharge, while mineral zoning patterns show evidence of magma mixing. These results demonstrate that moderate-intensity summit eruptions can exhibit complexities typically associated with maar-diatreme systems.

Keywords: Phreatomagmatic; Tephra recycling; Maar-like formation; Tuff cone; Magma mixing.

1 Introduction

The 25-month-long 1963–1965 Irazú eruption (Volcanic Explosion Index, VEI, maximum 3) was one of the best-documented volcanic events in Central American history, producing detailed contemporary observations, photographs, and scientific reports [**Waldron_1967**; Murata et al. 1966] that provide an exceptional framework for interpreting the tephra deposits. The eruption was initially classified as Strombolian [Murata et al. 1966] and later cited as typical "Vulcanian" activity [Walker 1973; 1981; Cas and Wright 1987]. Despite its low to moderate intensity, the eruption caused significant impacts due to persistent ashfall and lahars, highlighting the importance of understanding eruptive dynamics at this volcano for hazard assessment in the densely populated Greater Metropolitan Area (GMA) of Costa Rica.

Walker [1973] recognized that Irazú was the first volcano for which volcanologists mentioned the process which produced recycled clasts: "*In a typical explosion, the finer particles (<1 mm diameter) were carried away by the wind, while the coarser particles fell back into the crater to undergo further abrasion and fragmentation. By repeating this process, the volcano functions as a veritable rock crusher and dust machine. Periodically, part of the vent wall would topple to furnish more grist for the mill*" [Murata et al. 1966]. This process of tephra recycling has gained increasing attention in volcanology because it significantly affects eruption volume estimates, grain size distributions, and the interpretation of fragmentation mechanisms. Failure to recognize recycled clasts can lead to overestimation of juvenile magma volumes and misinterpretation of magma supply rates and eruptive dynamics, particularly in long-lasting eruptions where repeated explosions and crater evolution create optimal conditions for extensive recycling [**DOriano_2014**; Houghton and Smith 1993; Deardorff and Cashman 2017]. Juvenile fragments can be classified as primary juvenile clasts, involved in a single eruptive pulse, or recycled juvenile clasts, which were fragmented and ejected by an earlier explosion during the same eruption, but fell back or collapsed into the vent and were re-ejected [Houghton and Smith 1993]. Recycled clasts can be considered *cognate lithics* [**DOriano_2014**]. The efficiency of this recycling process at Irazú is reflected in the high degree of fragmentation (~85 %) estimated by **Wright_1980**.

Although the 1963–1965 eruption of Irazú occurred at the summit of a large andesitic shield volcano, the eruptive processes and resulting deposits share notable similarities with maar-diatreme systems [**Alvarado_1993**]. Prior to 1963, the Main Crater contained an irregular floor with several small pit craters and a volcanic terrace on its western side. During the eruption, the Active Crater (the main eruptive focus from 1963–1965) underwent significant enlargement in both diameter and depth, while a phreatomagmatic tuff cone developed on the western volcanic terrace. The resulting crater morphology, with its steep funnel-shaped geometry and surrounding tephra rim, closely resembles maar-like structures typically associated with phreatomagmatic eruptions at lower elevations or in different geological settings. This unusual development of maar-like features at the summit of a complex stratovolcano provides a unique opportunity to study crater-confined depositional processes, tephra recycling, and the interplay between magmatic and phreatomagmatic activity in a well-documented historical eruption.

* daniela.campos.duran@una.cr

[†] Passed away on August 24, 2024.

Previous studies of the 1963–1965 Irazú eruption focused primarily on narrative descriptions [Murata et al. 1966], lahar hazards [**Waldron_1967**; **Alvarado_1994**], tephra distribution [**Clark_2006**], and petrological aspects [**Alvarado_2006**; Ruprecht and Plank 2013; Oeser et al. 2018]. However, a comprehensive analysis integrating detailed stratigraphy, sedimentology, and depositional processes of the proximal tephra deposits has not been undertaken. This study aims to fill this gap by: (1) providing detailed stratigraphic descriptions of the intra-crater (ICD) and rim (RD) deposits; (2) interpreting depositional mechanisms based on sedimentological features and correlation with contemporary observations; (3) documenting the role of tephra recycling; (4) presenting new geochemical data that constrain the timing of magma recharge during the eruption; and (5) investigating the role of El Niño or Niña phenomena in aquifer recharge and phreatomagmatic activity.

This analysis should lead to a better understanding and broader awareness of the 1963–1965 eruption, whose details and significance remain poorly known even among volcanologists, despite being one of the best-documented historical eruptions in Central America. The results also have implications for hazard assessment at Irazú, one of Costa Rica's most hazardous volcanoes, which threatens the densely populated GMA.

2 Geological and geographic background

Irazú volcano (3427 m a.s.l.), an andesitic shield volcano in the Cordillera Central of Costa Rica, is one of the largest volcanoes (700 km^2, 359 km^3) along the Central American Volcanic Front (CAVF). It has been intermittently active over the past 0.6 Ma [**Alvarado_2006**; **Alvarado_2012**] and is located 155 km NE of the Middle America Trench, at the southern end of the CAVF (Figure 1A). An intermontane basin at about 1000–1200 m a.s.l., called Valle Central, exists between the Cordillera Central and the Cordillera de Talamanca. This basin includes GMA (home to nearly 60 % of the country's population, 3.3 million inhabitants), which is the economic and social center of the country. Most of its population resides in San José, the nation's capital (30 km west of Irazú), as well as in the nearby cities of Cartago, Heredia, and Alajuela and dozens of smaller towns and urban areas (Figure 1B and 2A).

The volcanic rocks of Irazú range from basalt to andesite and minor dacite and represent a calc-alkaline trend with an ocean island basalt (OIB)-like signature. The summit of Irazú features two major craters: Diego de la Haya Crater and the Main Crater (Figure 2B). Additionally, there is a cinder cone called La Laguna and Playa Hermosa, which is part of a large old crater or sector collapse caldera rim, contributing to the complex summit area of Irazú. The Main Crater is the focus of all historic volcanic activity (i.e. 1723–1724 and the 20th century). The summit of Irazú is covered by lava flows, Strombolian deposits, and phreatomagmatic tephra deposits laid down during the last 50 ka, but there is no evidence of Holocene Plinian eruptions. Approximately ten cinder cones and craters are present along fissure systems on the southern flank of the volcano as well as an E–W fissure that has been active during the last 2.6 ka, right where the Main Crater is located [**Campos_Dur_n_2024a**; **Campos_Dur_n_2024b**].

Irazú has been active throughout the Holocene, with the most recent eruptive phases occurring in 1723–1724, 1917–1921, 1924, 1928, 1930, 1933, 1939–1940, and 1963–1965 [**Alvarado_1993**; **Alvarado_2006**]. The 1963–1965 eruption was the largest and longest of these historical events. A comprehensive study of Late Holocene tephra deposits was recently presented by **Campos_Dur_n_2024b**.

2.1 Narrative of the 1963–1965 eruption

The early volcanic manifestations at Irazú began on August 9, 1962, with minor activity, principally as a vapor column. At the end of January and beginning of February 1963, strong scoria lapilli and ash eruptions were observed. Starting from March 1963, Irazú volcano experienced a vigorous eruptive phase accompanied by heavy ashfall on San José on March 12, 1963 (Figures 3A–3C). Three major explosions in rapid succession generated mushroom clouds of ash and incandescent bombs, which fell more than one kilometer from the crater. Ashfall was reported in Nicoya, 200 km west of the volcano, on March 12–14; this phase of the eruption culminated on March 14, with more than 8 h of quasi-continuous explosions and tephra ejection (Figure 3A). By early June 1963, three vents existed in the Main Crater [**Miller_1966**], and at least two were reported in October of the same year. One vent emitted mostly steam, another quietly ejected smaller particles at irregular intervals, and the third appeared to be responsible for the ejection of large blocks and produced a rumbling sound audible 25 to 50 km away [**Gawarecki_1980**]. The trajectories of the bombs become increasingly horizontal over time [Murata et al. 1966]. During the early mornings at the end of December 1963, when the Caribbean westerly wind had not yet started, ash clouds rose to a height of 11 km [**Gutirrez_1963**; **Cordero_1964**; **Miller_1966**; Murata et al. 1966]. Glowing lava was observed from mid-December 1963 to January 1964 and in May 1964, approximately 100 m below the crater rim [**Gawarecki_1980**; Murata et al. 1966].

The umbrella cloud region usually developed at 0.5–1 km above the crater. Finger jets ("cocktail jets" or "cypressoidal jets") shooting up from the crater to heights of hundreds of meters and lightning within the ash column were frequent during such times. Strong explosions commonly occurred after a period of relatively weak activity and propelled the ash column to heights of one kilometer or more [Murata et al. 1966]. The continuous uprush columns were incandescent overnight. In February 1964, bombs fell very near the Main Crater, but by June they were landing as far as 1.2 to 2.4 km beyond the crater rim [**Miller_1966**]. Eruptions were marked by deafening detonations, and, at night, the reverberations could be heard as faint rumbles even in San José, 24 km SW of the Active Crater. This type of activity (e.g. June 7, 1964) started with a sharp detonation, which generated an air shock wave that was felt a kilometer from the vent. The noise of the blasts reverberated, and ground vibration preceded the swarms of molten bombs that shot upward out of the vent; a few landed as far away as 700 m away. About two seconds later, a puff of white to tan steam would emerge from the vent.

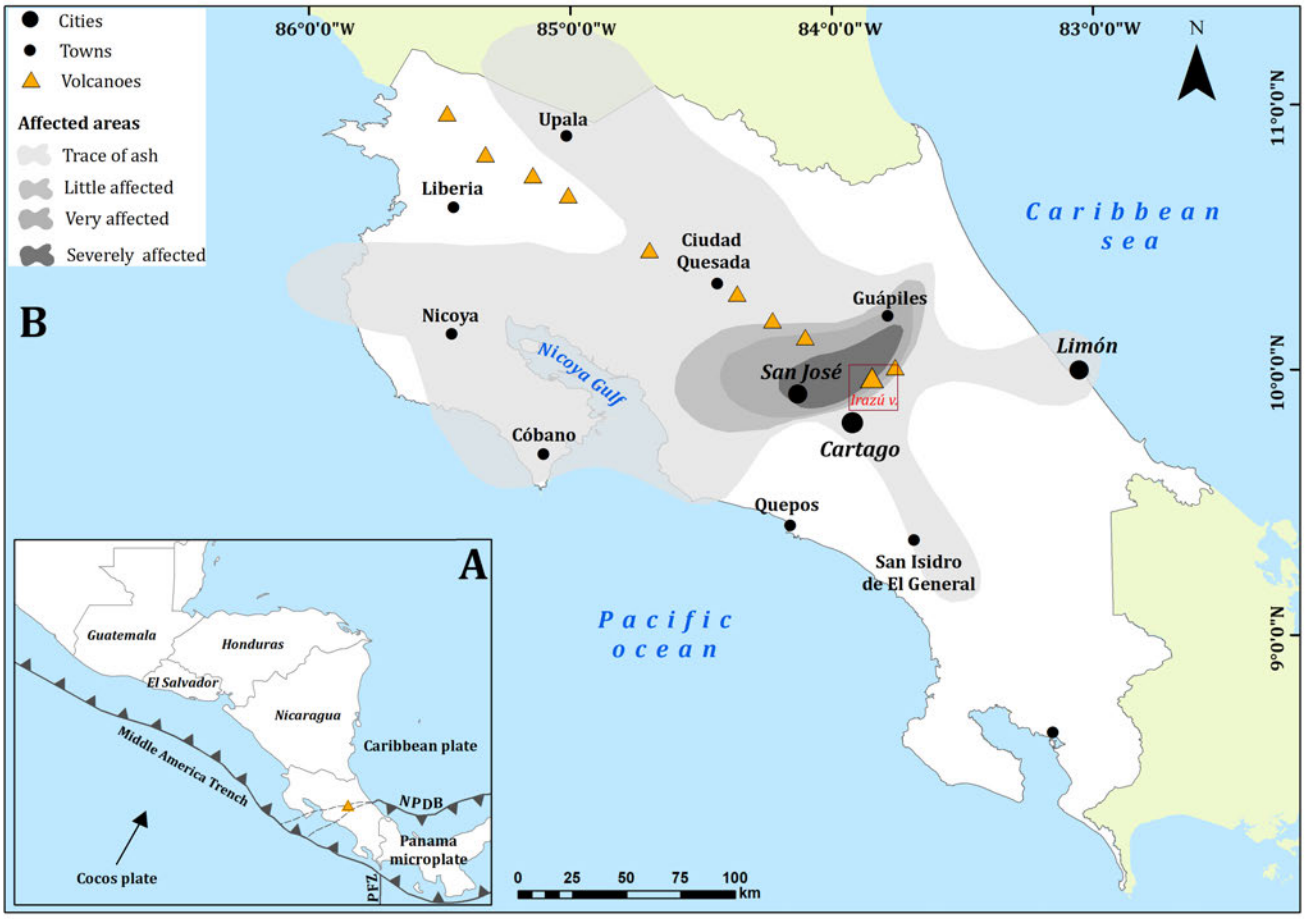

Figure 1: [A] General geotectonic framework of Costa Rica including the North Panama Deformed Belt (NPDB). [B] Distribution of volcanic ash from Irazú (1963–1965) and affected cities and towns (modified after **Co_n_1964**; **Barquero_1976**; **Gawarechi_1980**). The Irazú volcano is shown in the red box.

On August 26, 1964, eruptions of liquid water jets were observed concurrent with major rainfall events. Similar events occurred later, notably on October 26 and 27, 1964. The first days of November 1964 were marked by continuous eruptions of light-brown ash clouds and white vapor clouds. Four explosions of high black ash clouds accompanied by incandescent bombs, reverberations, and rumbling thunderous noise occurred on November 3. Nine days of relative quiescence followed, characterized by only low-lying (<0.5 km high) clouds of white vapor, until November 12, when a very strong, high, black ash-cloud eruption occurred, accompanied again by incandescent bombs and reverberations. Minor eruptions of low-lying steam clouds and ash continued with very short periods of inactivity or weak vapor eruptions at the end of November. Very strong eruptions were also accompanied by incandescent bombs, and on the night of November 27, an orange glow was observed in the crater. Low-intensity ash and vapor eruptions continued until December 29, followed by a series of dark brown to black ash clouds expelled to an altitude of 2.5 km above the rim of the crater [**Barquero_1976**; Murata et al. 1966; Krushensky and Escalante 1967].

Activity during January 1965 was variable, with periods of complete calm, ash cloud eruptions, or incandescent bombs and blocks, the latter without ash. Activity after January 25 was considerably reduced; the crater continued to emit low-lying light-brown ash clouds, steam, and rare blocks and bombs, alternating with periods of complete inactivity, particularly at the end of January. However, a strong explosion occurred on January 31. The last ash eruption of any discernible force was observed on the morning of February 13, 1965. By March 18, 1965, the crater completely lacked fumarolic or vapor activity [Krushensky and Escalante 1967].

The progressive enlargement of the Active Crater (that grew inside the old rim crater called Main Crater of 710–840 m diameter) during the 1963–1965 eruption was the largest morphological change at Irazú volcano since the 1917–1921 and 1924 eruptions, when several small pit craters coalesced [**Elizondo_2019**]. The 200-m-wide and 40-m-deep pre-1963 Active Crater became 450 m wide and 60 m deep in June 1963 [**Gutirrez_1963**] and was further enlarged to 570–680 m in diameter and 300 m deep. The crater has steep near-vertical walls, with a floor 140 m below the original level. The progressive growth of the vents resulted in a steep, 300-m-deep crater with an asymmetric funnel shape on the western side. Its current depth is approximately 270 m because it has been infilled by landslides and sedimentation.

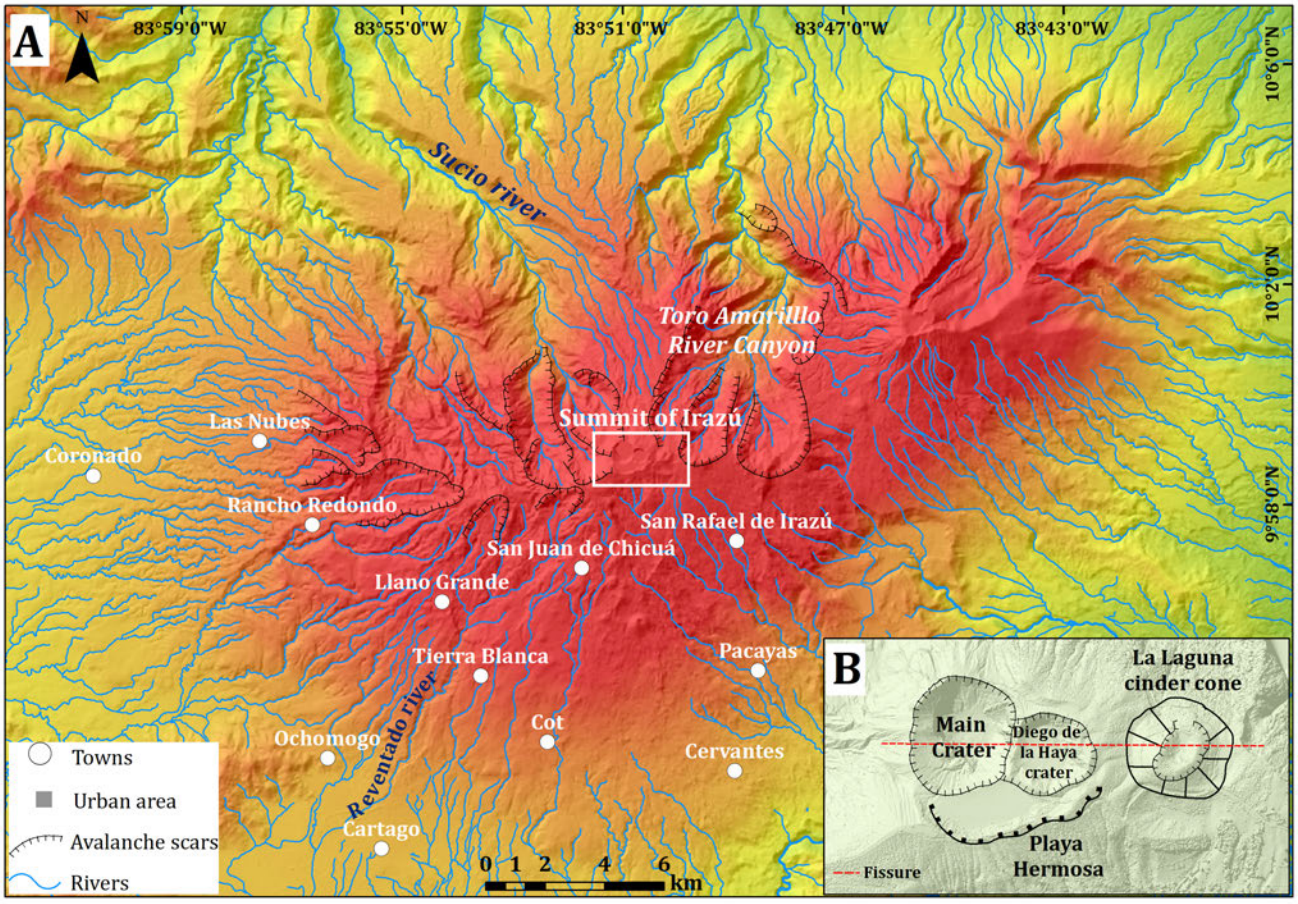

Figure 2: [A] Details of the flanks of Irazú, where lahars, volcanic debris avalanches, and landslides have been registered, mainly in the basins of the Reventado, Sucio, and Toro Amarillo rivers. [B] Digital Elevation Model of the summit of Irazú, showing its two craters and La Laguna cinder cone. The fissure proposed by **Campos_Dur_n_2024a** is also shown as a red dashed line.

3 Methods and materials

Most of the descriptions and sample collection were completed during three field sessions in 1990–1993 totaling 25 days, and mapping of the isopachs was complemented during the 2019 and 2020 field seasons (Figure 4A). In addition, three ash samples and two rock samples were collected in the field (Figure 4B) to estimate the bulk density of the material. The samples were analyzed at INSUMA S.A., a geotechnical laboratory in San José, following ASTM C127 (coarse aggregate) and ASTM C128 (fine aggregate) standards. Bulk density and open porosity were determined using the water saturation and hydrostatic weighing method: samples were dried at 110 °C to obtain dry weight, saturated in water to obtain the saturated surface-dry (SSD) weight, and weighed submerged in water to determine the apparent volume by Archimedes' principle. For methodological details, consult the aforementioned standards. These data provide the basis for estimating the Dense Rock Equivalent (DRE) and the volume of erupted tephra, following the formula:

$$\mathrm{DRE} = V \times \frac{\rho_d}{\rho_m} \quad (1)$$

wWhere V is the total volume of deposits (m^3), ρ_d is the average density of deposits ($g\,m^{-3}$), and ρ_m is the density of the liquid magma ($g\,m^{-3}$). To estimate the erupted volume, we examined 63 outcrops in Irazú National Park at medial distances (~6 km) along roads and artificial cuts for construction on the SW flank of Irazú and Valle Central (Figure 4A). Unfortunately, most of the 1963–1965 tephra deposits in Valle Central were quickly reworked and later removed for coffee plantation, urban, and industrial development. Consequently, we supplemented our fieldwork with reviews of historical documents, including journal articles, internal reports, newspapers, photographs, films, and theses, to better understand deposition and transport mechanisms. These data allowed us to construct an isopach map, which was the basis for estimating the apparent mass volume of the 1963–1965 eruption (see Supplementary Material 1).

Stratigraphically-controlled granulometric analyses of tephra samples in the interval −6 to 6.50 ϕ (64 mm–10 μm) were performed at the University of Bari (Italy), first using a set of sieves with half-ϕ intervals ranging from −6 to +3 ϕ (64–125 mm). After desiccation, the coarser material was hand-sieved to prevent breakage of vesicular fragments. Grain size analysis of the fraction finer than 125 μm was

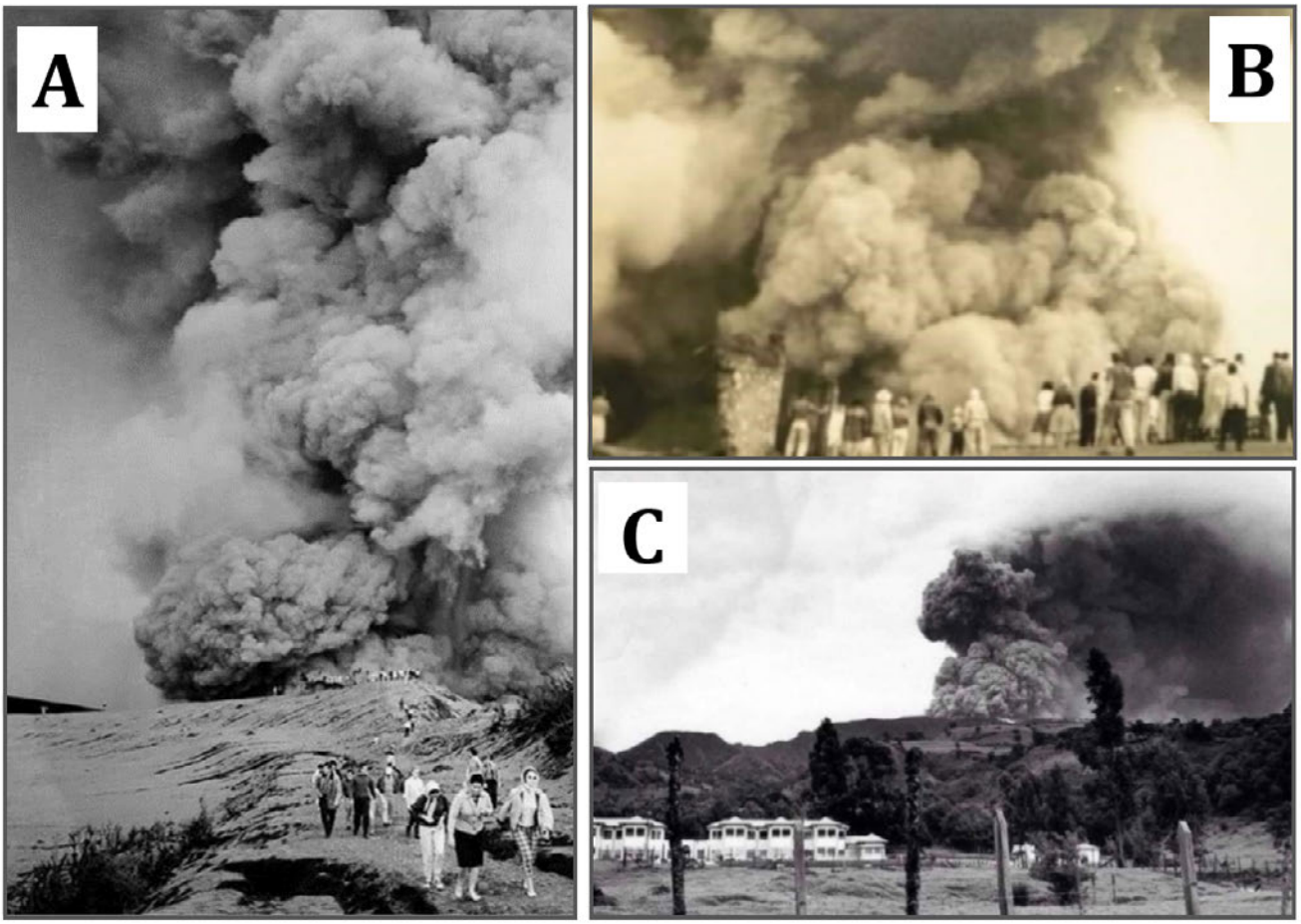

Figure 3: View of the Active Crater. [A] Example of a sustained plume of the sort formed by continuous uprush tephra columns on May 12, 1963. Residents and tourists at the crater rim at the moment of the eruption were frequent by day and by night (photograph by Francisco Coto). [B] The eruption of Irazú in March 1963 registered ash clouds affected by preferential winds (anonymous photograph, courtesy of Jorge Quirós). [C] Eruptive columns from the 1963–1965 eruptive period as seen in Sanatorio Durán with NNW directions of ash fall (anonymous photographs). Irazú's eruption became a great tourist attraction, as shown in these contemporaneous photographs.

performed using a Coulter Counter Ta II ° particle size analyzer, and the volume % output was converted into weight %, assuming a constant density for clasts <125 μm. Integrated complete grain size distributions with half ϕ intervals for all size fractions are reported as weight %, together with the conventionally used statistical parameter Md ϕ and sorting. We note that these two parameters are significant only in the case of Gaussian distributions, an assumption that is not met for many Irazú samples. However, these parameters are still useful when combined with a visual study of non-Gaussian distributions. The terminologies for the skewness parameter in the grain size distribution, class intervals suggested by Fisher and Schmincke [1984] for tephras on grade scales (millimeters or in ϕ units), and range of classification of sorting in pyroclastic deposits [Cas and Wright 1987, p. 473] were used.

Representative samples of the different types of deposits were selected for the stereomicroscopic study of the most representative grain-size classes to distinguish glass, lithics, and crystals [Sheridan and Wohletz 1983]. Subsequently, the particles were cleaned by a weak 30 second ultrasonic treatment in distilled water, which did not modify the original features of the clasts, and then their morphology was analyzed by scanning electron microscopy (SEM) using a Cambridge Stereoscan 360 system at University of Bari. Juvenile bombs and lapilli (n = 12 samples) were selected on the W and SW part of the Main Crater for thin section and modal analyses of the relative proportion of phenocrysts. Modal compositions (based on 18 modal analyses, expressed vesicle-free) were determined by point counting of 300 to 1000 points per section, depending on grain size. Phenocrysts are larger than 300 μm, while smaller grains are classified as microphenocrysts.

The database used for this study included 28 new chemical analyses of the 1963–1965 tephra deposits (the location is shown in Figures 6, 7 and 8) obtained by X-ray fluorescence (XRF) analysis on glass pellets using a Philips PW 1480 spectrometer measured at the University of Bonn and the Geomar in University of Kiel, both in Germany (see Supplementary Material 2). The analytical program Oxiquant with a calibration program for geological samples based on 270 synthetic

and international certified standards [**Govindaraju_1989**] was used in this study.

4 Results

4.1 Eruptive stages

A quantitative record of the ashfall of this eruption exists, as the monthly ashfall was reported by the Servicio Meteorológico in San José (at that time in the Museo Nacional), approximately 24 km downwind from the vent (ICE 1965, see Figure 5). Although this record is probably affected by the rainy season because rainfall near the volcano precipitated some of the ash before it reached San José, and ashfall was easily washed during heavy rain [**Coen_1964**; see comments in Murata et al. 1966], the amount of ash is plotted in Figure 5 as a cumulative curve. We tried to correlate this record with the chronological narrative presented in Section 2.1, and based on this, we identified four distinct eruption stages that are summarized in the following paragraphs. To our knowledge, this is the first formal subdivision of the 1963–1965 eruption into quantitatively defined stages based on ashfall accumulation data. Previous studies have not established a stage-based framework for interpreting the eruptive sequence.

- *Stage 1* was a period of relatively low activity, alternating with strong explosive phases from early February to December 9, 1963. Emission of ash and bombs was extremely abundant on the first day of the major open-conduit explosive activity (March 13, 1963), but activity thereafter settled down to intermittently ash-rich explosions (e.g. April, May, early July, and November 1963), bombs falling up to 7 km from the crater (e.g. November 16), and ash-poor steam. The greatest ashfall occurred on December 3, 1963, between 2 a.m. and 11 a.m. (local time: LT + 6 h = GMT), when 1248 g m^{-2} settled in San José. This marked the beginning of intense activity that continued until December 6 and gradually tapered off to modest activity by December 9. A pause in the eruption occurred during December 10–16, 1963, at the same time that an intense rainfall in the volcano region caused strong erosion. This period is probably represented in the stratigraphic section by several small erosional channels, which mark the boundary between sStages 1 and 2.

- *Stage 2* corresponds to the period of greatest activity, with extremely voluminous emission of scoria and bread-crust bombs that occurred between December 19, 1963, and the end of January 1964.

- *Stage 3* occurred between February and August 1964. The production of ash and bombs declined markedly after June 1964.

- *Stage 4* occurred between September 1964 and February 1965, during which the incandescent material continued to be ejected until at least January 1965. The last recorded eruption of non-juvenile blocks occurred on February 8, 1965, and activity ceased on the morning of February 13, 1965.

4.2 Stratigraphic sections and tephra deposits

Two representative well-exposed sections of the 1963–1965 tephra deposits located in the summit area of Irazú were studied to attempt to reconcile the narrative and geological records of the 25-month eruptive period (Figures 6, 7, and 8 for location). The first step was to correlate the detailed sample collection of the 28-m-thick stratigraphic column present in the internal wall and floor of the Main Crater (Figure 6), called intra-crater deposits (ICD), which forms a part of the asymmetric tuff ring built on a pre-existing intra-crater terrace (western part of the Main Crater).

The second section comprises tephra deposits (≤ 5.7 m, Figure 7) in the surrounding craters of Irazú, which we refer to as rim facies (RD). The deposits are not indurated. The RD sequence represents about 80 % of the thickness reduction in a few hundred meters due to the topographic barrier of the Main Crater walls with a difference of ~90 m in elevation and the prevalent eastern-northeastern wind direction that limits the ICD in the RD deposition region. Thus, the ICD pinched out laterally to the RD. The ICD shows considerably more stratigraphic and structural complexity than the RD deposits (Figures 6 and 7), which is also evident in ground-penetrating radar images [Kruse et al. 2010]. Although it is difficult to correlate individual layers or units between these facies, the proportions of the deposit types were similar (see Table 1). Correlation between the ICDs on the western side and the RDs on the southwestern side is challenging due to several factors: (1) the two sites are separated by ≤90 m in elevation; (2) they have contrasting morphologies (rough, irregular terrain for ICD versus flat terrain for RD); and (3) they experienced differential erosion by rainfall. Nevertheless, unconformities, rock chemistry, and a few distinctive tephra beds allowed correlation between ICD and RD.

Tephra deposited >4 km from the summit area has been largely reworked into soils by recent agricultural activity and mixed with anthropogenic debris, particularly near towns, cities, farms, and road cuts, or is covered by dense forest and grass. The distal deposits were not preserved in the stratigraphic record on land because only traces of ash were deposited more than 25 km away.

4.2.1 *Intra-crater deposits (ICD)*

On the western and downwind sides of the Main Crater, a 14- to 32-m-thick section represents a complete record of the 1963–1965 eruptions. The ICD rest on a steep and irregular contact that represents the paleosurface of a pre-1963 Irazú crater (Figure 6 and Figure 8A for location). The pre-1963 substratum is dominated by indurated, poorly-sorted volcanic breccias, tuffs and agglomerates, which are geochemically different from the 1963–1965 tephra deposits [**Alvarado_2006**]. Pyroclastic deposits emplaced during 1963–1965 eruption range from bedded to cross-bedded tuffs and lapilli tuffs, massive tuffs, rare breccias, abundant ballistic clasts, and post-eruptive sediments (i.e. colluvial, landslides, sheets, and granular flow deposits) (Figure 6).

The deposits are fan-shaped, and the beds dip into the crater at 23–30° near the internal slope rim of the Main Crater and 0–2 ° near the Active Crater. Dips larger than 15 ° were

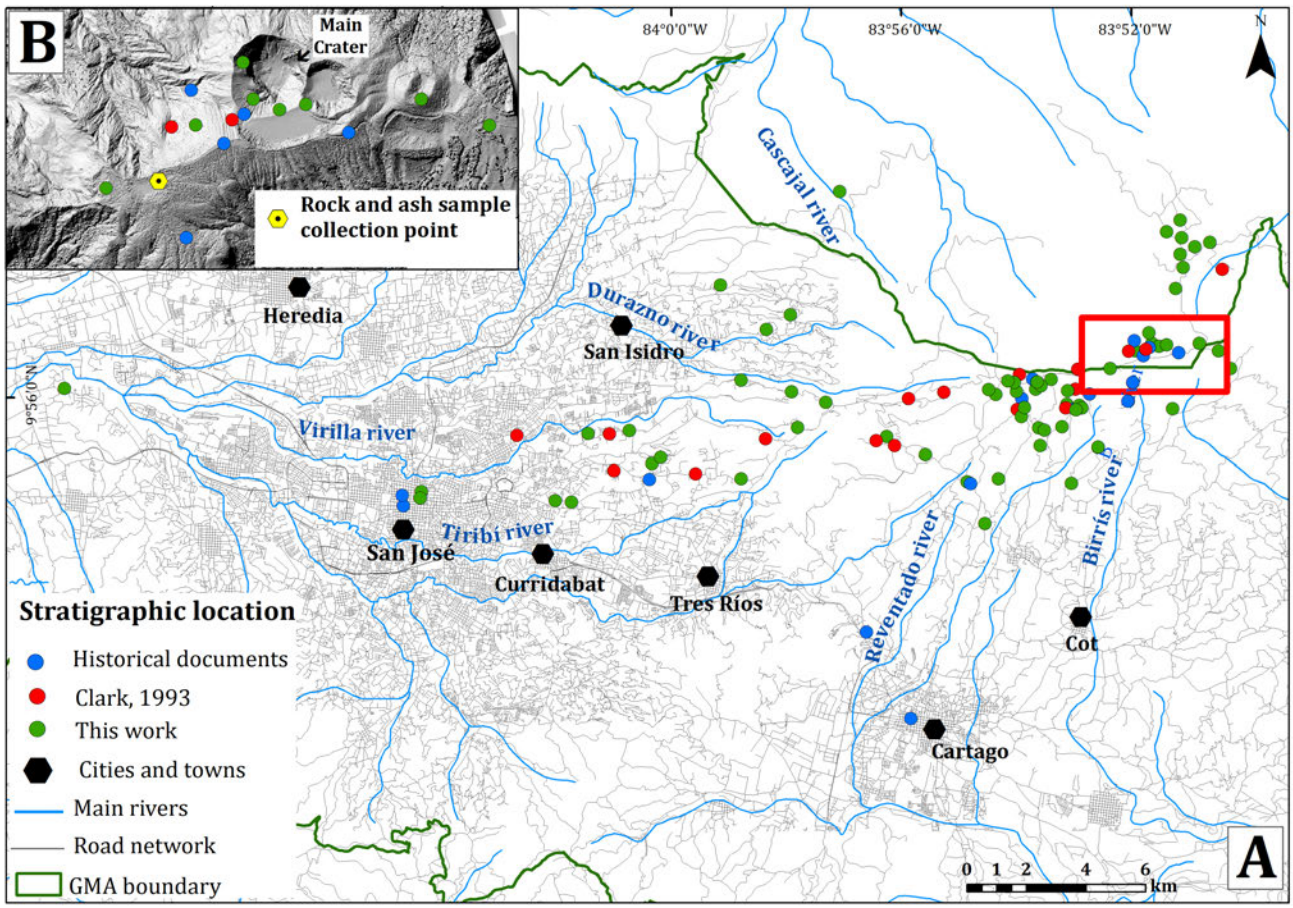

Figure 4: [A] Location of stratigraphic sections for the 1963–1965 tephra deposits. Stations include: this study (n = 63, green circles), Clark_1993 data collected between 1990–1993 (n = 17, red circles), and historical measurements compiled from contemporaneous reports and photographs (n = 16, blue circles); see Supplementary Material Table S1 for sources. The red rectangle delimits the summit area shown in panel B. The Greater Metropolitan Area is located to the southwest of the summit; the main city (San José) is located approximately 25–30 km from the summit. [B] Detailed map of the summit area showing location of ash and rock samples collected for density measurements (yellow hexagon), and the crater morphology. Geographic Coordinate System. Due to scale constraints, some data points may appear superimposed.

Table 1: Comparison between ICD and RD.

	Facies	Predominant grey ash beds with large juvenile blocks and bombs	Brown ash and lithics beds	Scoriaceous deposits (lapilli to bomb/juvenile blocks)	Reworked tephra
ICD	Thickness (m)	22.4	1.1	4.7	3.6
	Approximate %	70.4	3.5	14.8	11.3
RD	Thickness (m)	4.8	≤ 0.02	≤ 0.15	≥ 0.7
	Approximate %	84.5	0.35	2.5	12.65

produced because the tephra was deposited on a pre-existing irregular floor and wall crater morphology. Depending on the location, a high angle (>30°) to low angle unconformity with a relatively smooth erosional shape marks the contact with the pre-1963 tephra sequences exposed in the Main Crater. Individual bed thickness varied from a few centimeters to about 1.5 m and ranged from massive to finely stratified coarse ash beds, and the granulometry varied from fine ash to bombs up to 2 m in diameter. Lithics (hydrothermally altered or unaltered) are angular to subrounded, all derived from the previous volcanic sequences (wall-rock lithics, ≤10 %), and easily recognized from the juvenile blocks due to the color (orange, brown, light grey), without fresh glassy surface or greasy luster. Juvenile clasts range from highly vesicular scoria lapilli and bombs to non-vesicular clasts (compact bread-crust bombs). Bombs (usually ≤0.5 m diameter) are oval or elongate, black to yel-

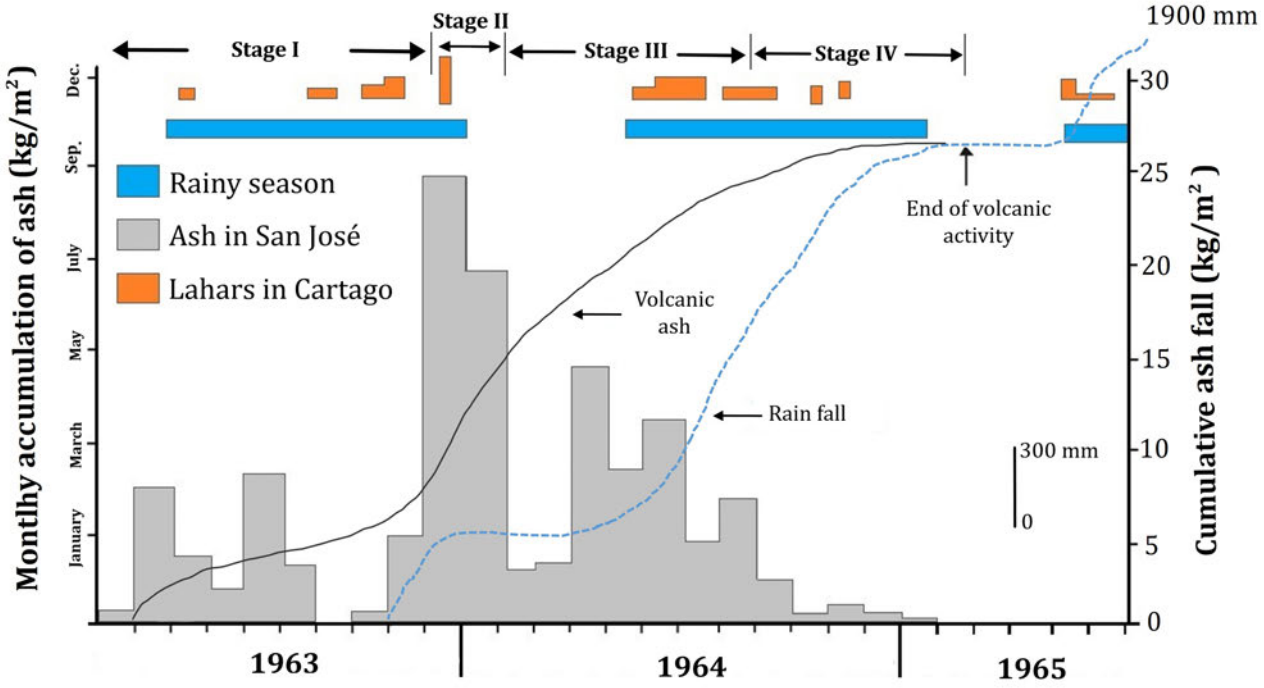

Figure 5: Monthly accumulation of Irazú volcanic ash on San José from March 1963 to February 1965 [ICE_1965] and the four stages of volcanic activity based on the curve analyses and the narrative of the eruption. Orange bars indicate the major lahar events at the Reventado River and their relative intensity. No rainfall data is available before October 1963.

lowish, and some are reddish-black due to extensive oxidation. Juvenile blocks have greasy black luster. There were also some isolated large bombs and blocks (1–2 m in diameter).

The first explosive layer in the ICD is a block- and bomb-bearing coarse deposit (≤1.7 m thick). The first 10 cm is a juvenile-bearing coarse ash layer with scattered hydrothermally altered lithics. The larger bombs (50 × 30 × 25 cm) are black to yellowish (some with a red exposed surface). Hydrothermally altered lithics are between 10 and 50 cm in diameter while non-hydrothermally altered lithics are present in the upper part, poorly reversely graded. Throughout the entire sequence, abundant thin scoria lapilli layers (7–30 cm thick) are present; however, block- and bomb-bearing layers (up to 2.5 m thick) occur principally in the lower section. Some layers are composed almost entirely of coarse-grained spindle bombs, fragile bombs, and finer-grained black scoria lapilli; lithic clasts are rare (0–5 %). The scoriaceous lapilli and bombs are coarse-grained, not always well-sorted, and display an asymmetric Gaussian grain size distribution (e.g. samples Ira 2/3 and 2/5, Figure 8). Fine-ash material infills the pore spaces in the clast-supported bomb and lapilli beds.

A consolidated gray tuff (25 cm thick) with desiccation fractures is present at about 2.5 m upward from the base (Figure 6). It is covered by interbedded, thinly laminated ash (15 cm thick) with cross laminations and a thin layer of scoriaceous lapilli. Throughout the tephra sequence, only a few finely laminated gray-brown layers occur (3–11 cm thick); one of these contains accretionary lapilli (7–8 cm thick) and is located about 11 m from the base. Most infrequent are the deposits consisting of hydrothermally altered and unaltered lithics (diameter ≤20 cm), and rare juvenile blocks and bombs in a brown-orange muddy ash with sag structures (20–36 cm thick), some of which contain an erosive contact in the lower part. Several layers are composed of cross-laminated ash, medium to well sorted with isolated lithics, usually overlain by a poorly laminated to massive ash bed with isolated lithics. Interbedded there is a lapilli-bearing ash with a 6-cm-thick, grey-brown vesicular tuff. It is overlain by a brown-ash layer with hydrothermally altered blocks, juvenile blocks and scoriaceous bombs and lapilli in a finely laminated (parallel and perturbed) brown-ash and bomb-sag structure; the lower part is an erosive contact (see Figure 6).

The ICD shows numerous high- to low-angle internal unconformities due to syn-eruptive landslides as well as "U"-shaped rills that are interpreted to have formed by surface runoff of heavy rain that was very frequent during the eruption, particularly during the rainy season (between May and December) of both years, 1963 and 1964. An irregular contact at the base of one slide block (~1.9 m thick) consists of ash beds with blocks and chaotic internal structure (i.e. vertical and discontinuous beds, flow-folded structures, and irregular contacts), and one scoria lens. These features indicate that this slide was formed by syn-eruptive collapse of the growing crater. Well-developed syn-depositional removal of ash-laden slurries occurred via slumping on steeply dipping slopes

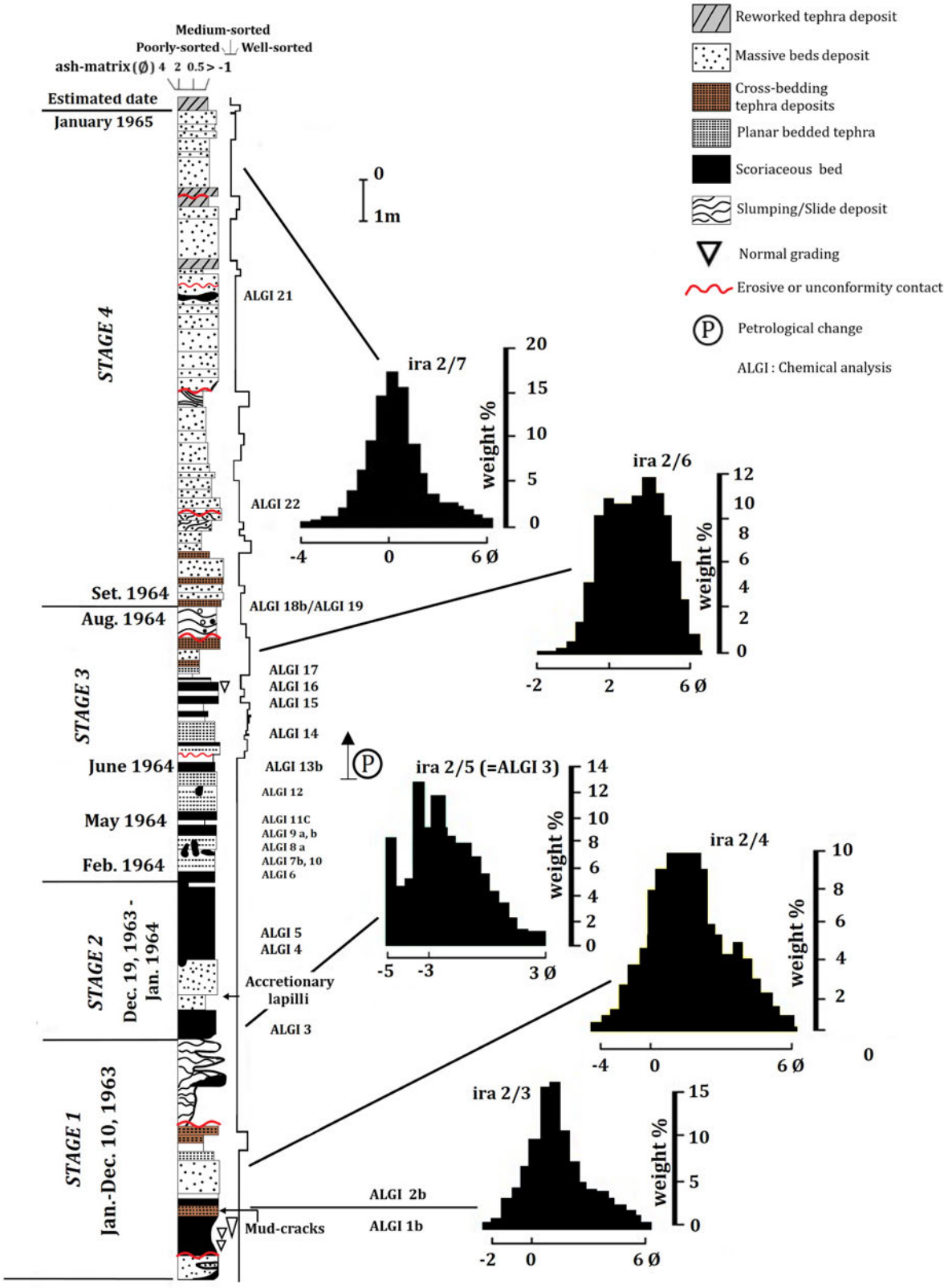

Figure 6: Generalized stratigraphic section showing the complex eruption sequence of the 1963–1965 tephra eruption at the intra-crater deposit (ICD) and representative grain size (Ira samples) data, and indication of rock samples used for chemical analysis (called ALGI). The circled (P) is the main petrological change described in the text. The location of this column is shown in Figure 8.

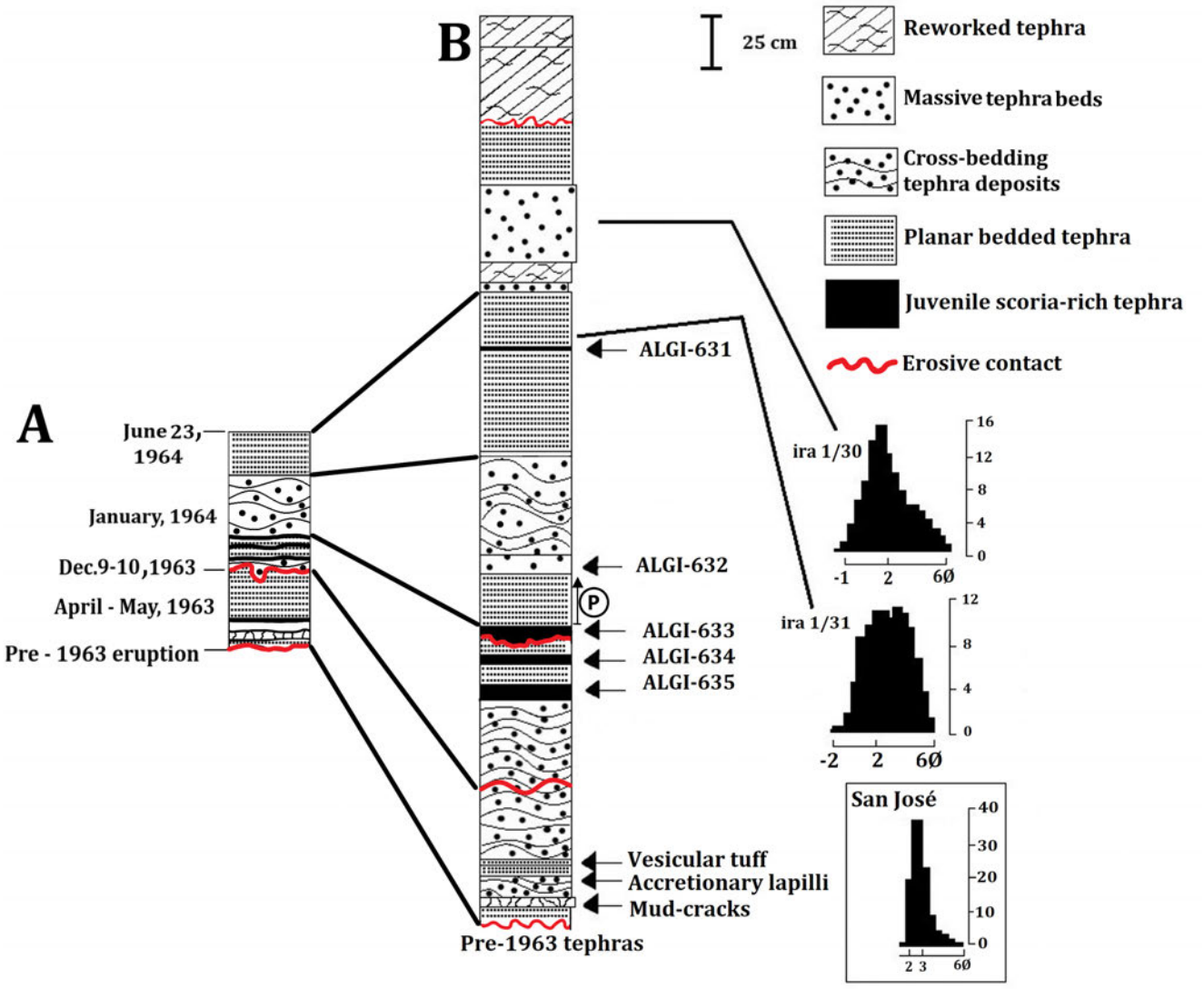

Figure 7: Generalized stratigraphic section at rim deposit (RD) at the present time [B], and its correlation with an incomplete stratigraphic section (1.7 m thick) described by Murata et al. [1966] in 1963 [A]. The San José sample (grain size) was taken at the capital (San José) and represents the medial facies at 24 km SW from the vent. The prominent erosional surface was interpreted as the result of a huge downpour on December 9–10, 1963. See Figure 8 for the location of the columns. Representative grain size (Ira samples) data, and indication of rock samples used for chemical analysis (called ALGI). The circled (P) is the main petrological change described in the text. The location of this column is shown in Figure 8.

within the southwestern crater. This penecontemporaneous soft-sediment deformation occurred in water-rich tephra deposits. At least eight major erosional contacts were observed in the ICD (Figure 9).

About 35 massive units can be distinguished in the ICD, particularly in the upper half of the outcrop (Figure 9A). These horizons are characterized by predominantly massive ash beds (5–100 cm thick), consisting of fine-grained, non-cohesive, poorly- to moderately-sorted ash. The ash is made up of broken and unbroken crystals and lithoclasts of uncertain origin (either juvenile or reworked) with little or no internal layering. Massive beds commonly contain randomly scattered lapilli to large blocks (usually <3 cm; maximum 20 cm). Imbricate structures (usually oriented towards the crater floor) are the only fabric evident in these minor units. There are also bomb-sag structures on the top of the massive ash beds; however, most accidental blocks into the massive ash deposits lack pronounced sags. The units have a sharp, commonly erosive base, and show either normal or no grading. A relatively fine-grained, cross-laminated basal layer, ranging from a few centimeters to less than 10 cm thick, is a common feature of this facies. Some beds were composite, and layering was marked by the presence of thin, laterally discontinuous coarse ash and lapilli lenses. The thickness (10–45 cm thick) of these composite beds varies considerably over short distances, displaying pinch-outs in the downstream directions or towards the crater floor.

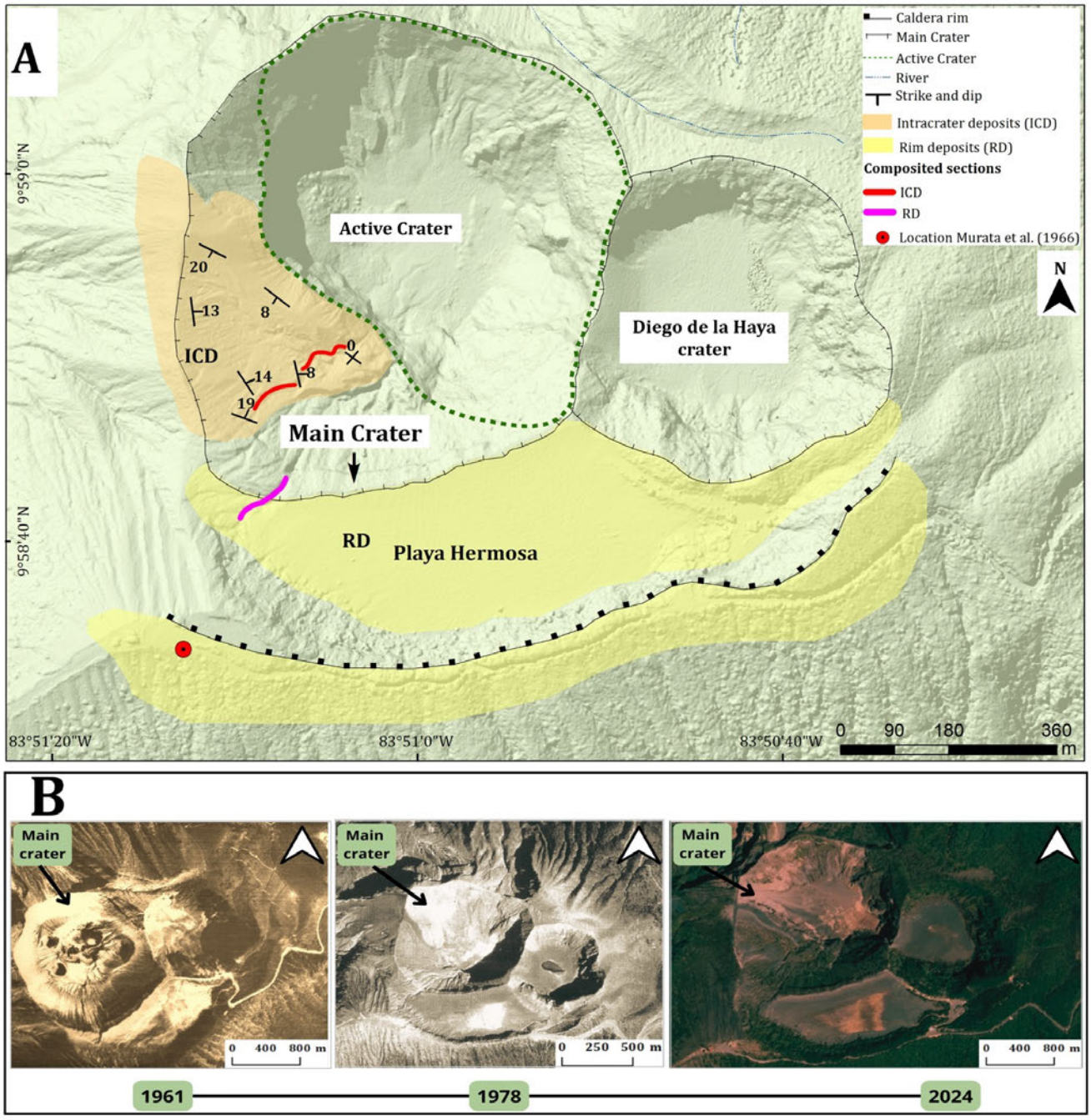

Figure 8: [A] Crater structures of Irazú. Playa Hermosa is an old caldera rim, Diego de la Haya is a dormant focus, and Main Crater is the old morphological crater and the foci of historical eruptions, but the Active Crater is the enlargement of the previous foci generating what we call the Active Crater. The intra-crater deposits (ICD) and the composite stratigraphic section (Figure 6) are part of an asymmetrical tuff cone, whereas the rim deposits (RD) (composite stratigraphic section, see Figure 7) are thinner and present mainly on flat topography. The historical stratigraphical section (June 23, 1964) from Murata et al. [1966] was located near the highest point of Irazú. [B] The morphology of the Main Crater of Irazú prior to the 1963 eruption, 15 years post-eruption, and present morphology. The ICD developed on the floor and western wall (volcanic terrace) of the Active Crater.

4.2.2 *Rim deposits (RD)*

In the RD, the 1963–1965 tephra sequence (up to 5.7 m thick; Figures 7 and 8A) rests on the erosive contact with the 1723–1724 tephra deposits and thin early 20th century tephra layers. These historical deposits (i.e. 1723–1724 and 20th century tephras) are absent in the ICD, where they were removed by erosion. These pre-1963 historical tephras are geochemically, petrographically, and mineralogically distinct from the 1963–1965 deposits [**Alvarado_1993**; **Alvarado_2006**]. The RD starts with a massive grey bed (10 cm thick) of fine ash with plant remains. Above this, a mud-cracked horizon (3–3.5 cm thick) lies, overlain by a brown layer of accretionary

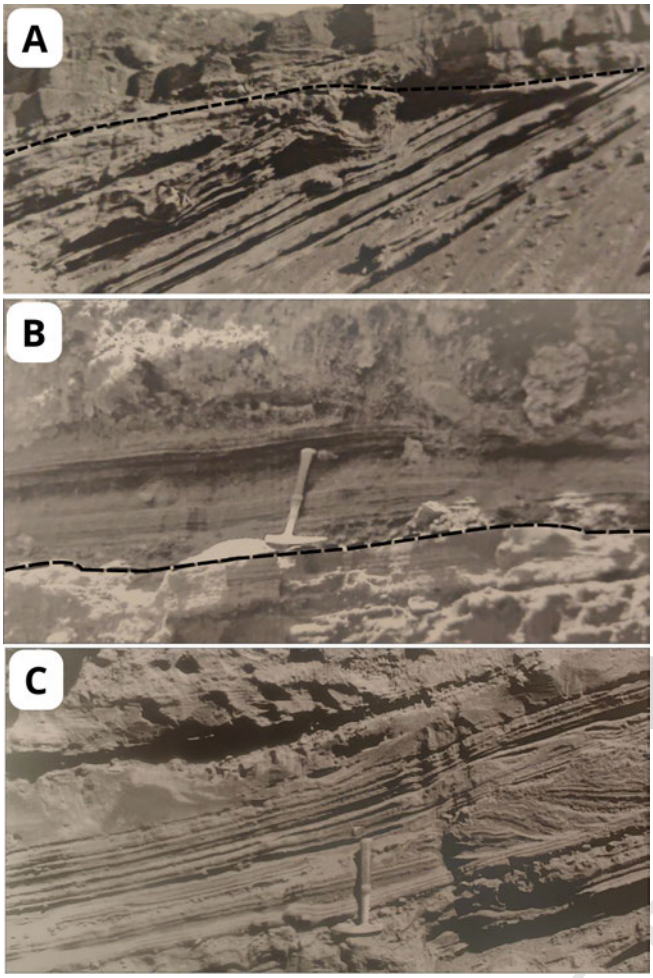

Figure 9: Photographs of the intra-crater deposit (ICD): [A] Slide surface sloping into the Main Crater. Late massive pyroclastic deposits from Stage 4 were deposited on the slide surface. [B] The hammer shows where the 1963-1965 tephra deposits (planar bedded and ballistic bombs deposits) overlie the prehistoric tephra deposits in ICD. [C] Contorted stratification (penecontemporaneous slumping) between planar bedded deposits.

lapilli (1.5 cm thick). Four distinctive scoria and coarse ash beds with rare lithics (hydrothermally altered clasts, usually <1 cm in diameter) are present, varying widely in thickness (2–11 cm thick). Finely laminated gray ash with rare juvenile scoriaceous lapilli and several multi-colored (yellow, gray, brown) and finely laminated layers present, mantling the topography (Figure 10). Low-angle lamination (ripples), pinch-and-swell structures, and relatively well-sorted deposits that thicken in depressions, are also present. Both laminated and cross-laminated ash horizons are abundant in the lower half of the section. Very finely laminated ash mantles cross-laminated horizons and vice versa. In several cases, their upper surfaces are deformed by sag structures. A single massive fine-grained ash deposit (22–40 cm thick), similar to that observed in the upper part of the ICD, is present in the RD. Finely stratified tuff layers (some containing vesicles) are plastered on upright tree trunks in the RD near the Playa Hermosa rim. Additionally, bedded ash deposits a few centimeters thick are plastered wallpaper-like on the Diego de la Haya crater wall.

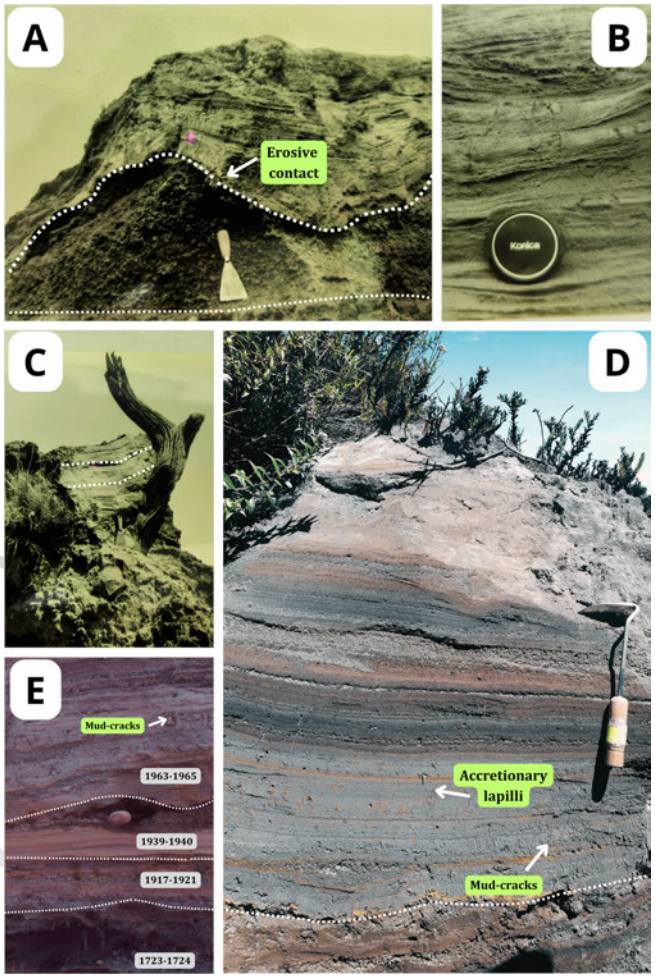

Figure 10: Photographs of the rim deposit (RD): [A] Erosive contacts between 1963–1965 stratified tephra deposits that overlie the 1723 scoria lapilli deposits. [B] Cross and planar bedding deposits plastered against the Diego de la Haya crater wall. [C] Pyroclastic deposits plastered again the base of the tree trunk. Note that the deposit climbs against the side of the trunk facing away from the Main Crater, which is about 250 m to the right. [D] Cross and planar bedding deposits, with small coarse ash layers, including the mudcrack layer. [E] Detail of the contact of the deposits of the first half of the 20th century and with those of the 1963–1965 eruption. Historical eruptions with stratigraphic correspondence are also shown.

4.3 Grain size distribution analyses and SEM results

The fine-grained and well-sorted fine stratified deposits usually have a Gaussian grain size distribution attesting to effective selection during transport. All massive deposits are relatively fine-grained and well to poorly sorted (ϕ = 1.35–2.2), while poorly sorted deposits display a bimodal distribution (Table 2). In the bimodal (poorly sorted) deposits, the two grain-size populations have different proportions of components. The coarse grain size mode (between -4 and 0 ϕ) of the massive deposits consists almost entirely of unaltered lithic

Table 2: Grain size parameters of representative tephra deposits.

Inman parameter	Scoria lapilli deposits	Massive ash beds	Non-cohesive ash deposits	Cohesive ash deposits	Distal ash
Md ϕ (mm)	−2.56	0.51–1.60	1.25	3.12–3.15	2.9
ϕ	1.93	1.35–2.2	1.65	1.62–1.64	0.63

fragments composed of basaltic andesite and older basaltic lavas characterized by variably rounded to angular shapes. These lithics are morphologically and chemically distinct from the juvenile clasts, displaying rounded forms and non-glassy surfaces (Figure 11). In contrast, the main part of the fine ash mode (between 0 and 6 ϕ) is composed of juvenile fragments showing a wide range of microscopic characteristics, as shown in SEM images (Figure 11). These features include blocky morphology with variable degrees of vesicularity, planar and curviplanar surfaces, and hydrated and quenched cracks, even in the internal parts of the vesicles.

4.4 Isopach map, volume, and volcanic explosivity index

The 1963–1965 proximal tephra deposits were rapidly channeled in several areas by erosion, while more distal ash was removed by runoff and mass waste in several sectors. A few studies have reported ash thickness reduction in several localities during and after the eruption [**Parsons_1967**; **Waldron_1967**; **Barquero_1976**; **Gawarecki_1980**; **Young_1998**; Murata et al. 1966]. The first isopach map was obtained in 1993, 28 years after the eruption [**Clark_1993**; **Clark_2006**]. It represents minimum values in several places because the mapped and measured sections are often thinner than those reported at the time of eruption owing to erosion and compaction. There are also several contradictions in the little available data; for example, in San José, **Waldron_1967** reported 2.1 cm, Gawarecki et al. (1980) about 8 cm, and Clark et al. (2006) reported an isopach thickness of less than 5 cm for the same eruption period. We complemented this information 48–56 years after the eruption with 63 new stations and corrected the isopach curves for the few measurements taken at the time of the eruption (Figure 12). In addition, we included in the volume estimates the 14–28 m thick tephra deposit of the 1963–1965 tuff ring in the ICD on the western inner wall crater (Figures 4 and 9).

Based on an exponential linear regression of the log thickness of isopachs, the previous estimate for the volume of the 1963–1965 event was 3×10^7 m^3 [**Clark_2006**]. Here, we integrated all previous datasets and the newly obtained information on tephra thickness. Our estimate for tephra volume is nearly double ~6.2×10^7 m^3. Regarding the apparent density of the material, we obtained five measurements: 2.64 g cm^{-3}, 2.51 g cm^{-3}, and 2.56 g cm^{-3} for the ash, and 2.37 g cm^{-3} and 2.75 g cm^{-3} for the rock (with an average of 2.56 g cm^{-3}); we also assigned a magma density of 2.8 g cm^{-3}, which is a standard reference value for basaltic to basaltic-andesite magmas [**Murase_1973**; **Spera_2000**]. This value is consistent with the composition of Irazú magmas (53.7–55.1 wt.% SiO_2) and is widely applied in tephra volume studies [e.g. Cas and Wright 1987]. Although a slightly lower density (2.5–2.7 g cm^{-3}) might be more specific for basaltic andesites, the choice of magma density introduces minimal uncertainty (±3–5 %) compared to other sources of error in volume estimation, such as isopach interpolation (±30–40 %). These data allowed us to obtain a DRE volume of ~5.68×10^7 m^3.

Considering the eruption duration (25 months), column height (8–11 km), and volume (5.68×10^7 m^3), we derived a volcano explosivity index (VEI) equivalent to 3, which is in good agreement with previous determinations [**Alvarado_1993**; **Clark_2006**; **Campos_Dur_n_2024b**].

4.5 Petrography, mineralogy, and geochemistry

Irazú ejecta are classified as high-K basaltic andesite (53.7–55.1 wt.% SiO_2) with unusually high concentrations of incompatible elements and Cr and Ni, a geochemical signature that is uncommon for basaltic andesites and provides evidence of magma mixing. The juvenile components contain 12–34 vol. % of phenocrysts comprising plagioclase ($An_{46\text{-}78}$: 9–30.2 %), pyroxenes (1.5–7.5 %; augite: $Wo_{33\text{-}42}En_{44\text{-}54}Fs_{8\text{-}18}$ + ferrosilite: $En_{70\text{-}78}$), and olivine ($Fo_{70\text{-}91}$ 0.4–2.0 %). Based on thin sections of juvenile rocks taken from the ICD, the phenocryst content is lower (27.6–33.6 %) in the first two stages (i.e. January 1963 to January 1964, Figure 7) compared with the latter two stages (35.0–39.7 %). Some normally zoned olivine crystals ($Fo_{71\text{-}91}$) contain picotite and rare titanomagnetite inclusions and often display an augitic corona ($Wo_{35\text{-}42}En_{45\text{-}51}Fs_{7\text{-}20}$); other MgO-rich olivines are poorly zoned ($Fo_{87\text{-}90}$) and without a clinopyroxene rim. Rarely olivines (no microprobe information) show an orthopyroxene rim with Fe-Ti oxides having a lamellar structure (symplectite-texture), occasionally associated with plagioclase. The microphenocrysts are opaques (mainly titanomagnetite, 0.1–1.7 %) and rare apatites. The groundmass (66–88 %) has the same mineral assemblage, except for rare olivine and orthopyroxene, set in a glassy andesitic to dacitic (SiO_2: 59.5–64.7 wt.%) groundmass. Glomerophyric clots consisting of cpx + opx + plag + mt + glass ± ol have also been found in juvenile bombs and blocks. The vesicles (<12.3–51 %) were round to subspherical.

Zoned and unzoned plagioclase phenocrysts coexisted in the same sample within the same size interval. Zoning patterns can be normal or reverse, with gradual compositional changes. Small microphenocrysts are $An_{35\text{-}52}$ in composition. Plagioclase phenocrysts were grouped into two types. Type 1 is characterized by the general absence of dusty or cellular textures and overgrowth. Clean and uniform crystals can be twinned and show limited internal zoning patterns (<5 mol. % anorthite content). Compositional range among different crystals was slightly larger at $An_{45\text{-}55}$. The largest phenocrysts in all samples were almost exclusively of this type. They

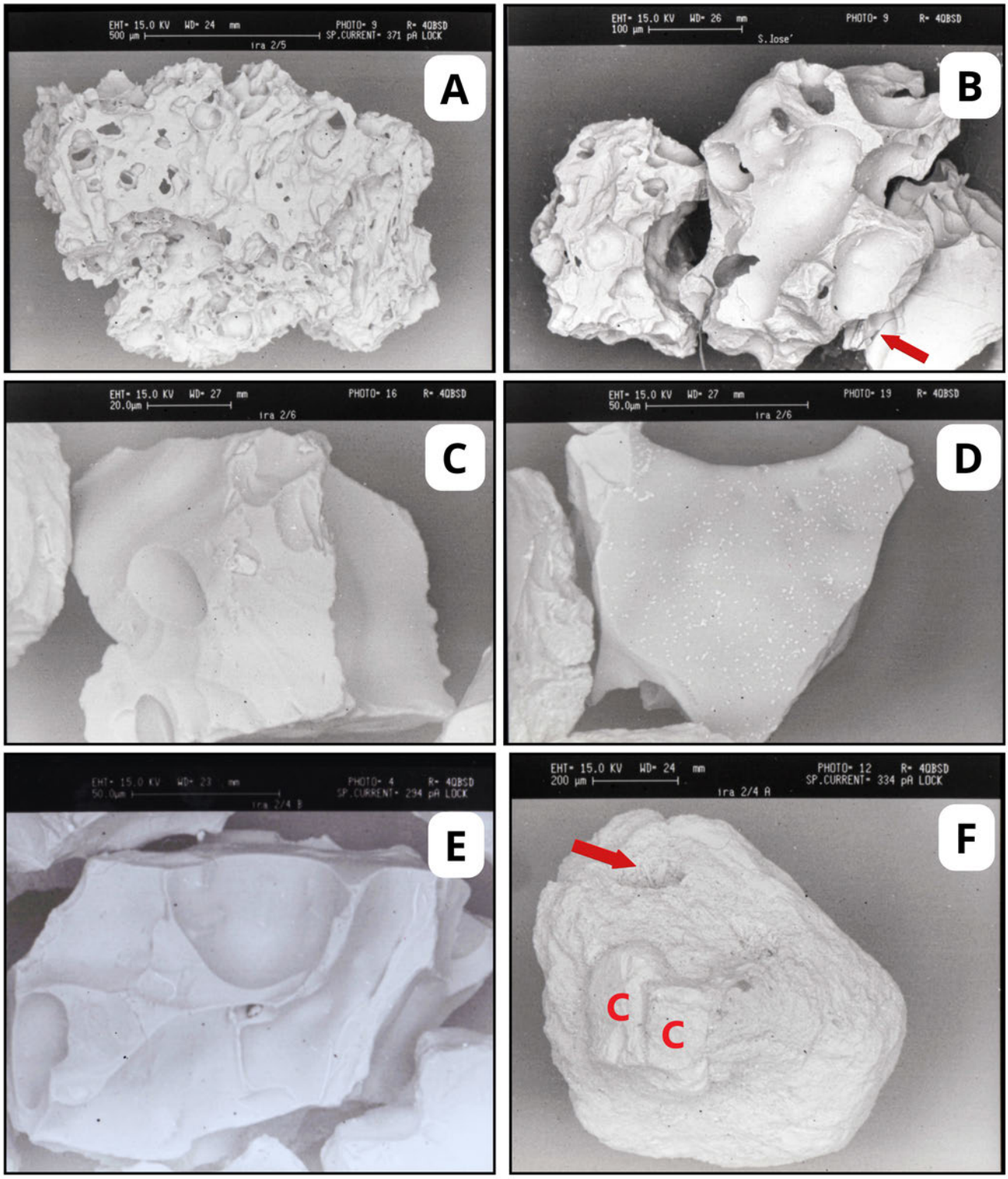

Figure 11: Scanning electron microscope images of ash deposits: [A] Scoria grain with abundant vesicle surface, irregular slopes, and jagged outline, typical of the bomb layers. [B] Juvenile grains with many broken vesicles and quench cracks (red arrow) from ashfall. [C] Juvenile low-vesicular equant blocky clasts from cross-bedding tephra deposits. [D] Juvenile low-vesicular blocky clast from cross-bedding tephra deposits. [E] Glassy low-vesicular juvenile blocky clast from dense pyroclastic density current. [F] Typical non-juvenile basaltic (round lithic) particle with mafic crystals (c) in a glass matrix from the massive tephra deposits, with possible impact structure (red arrow).

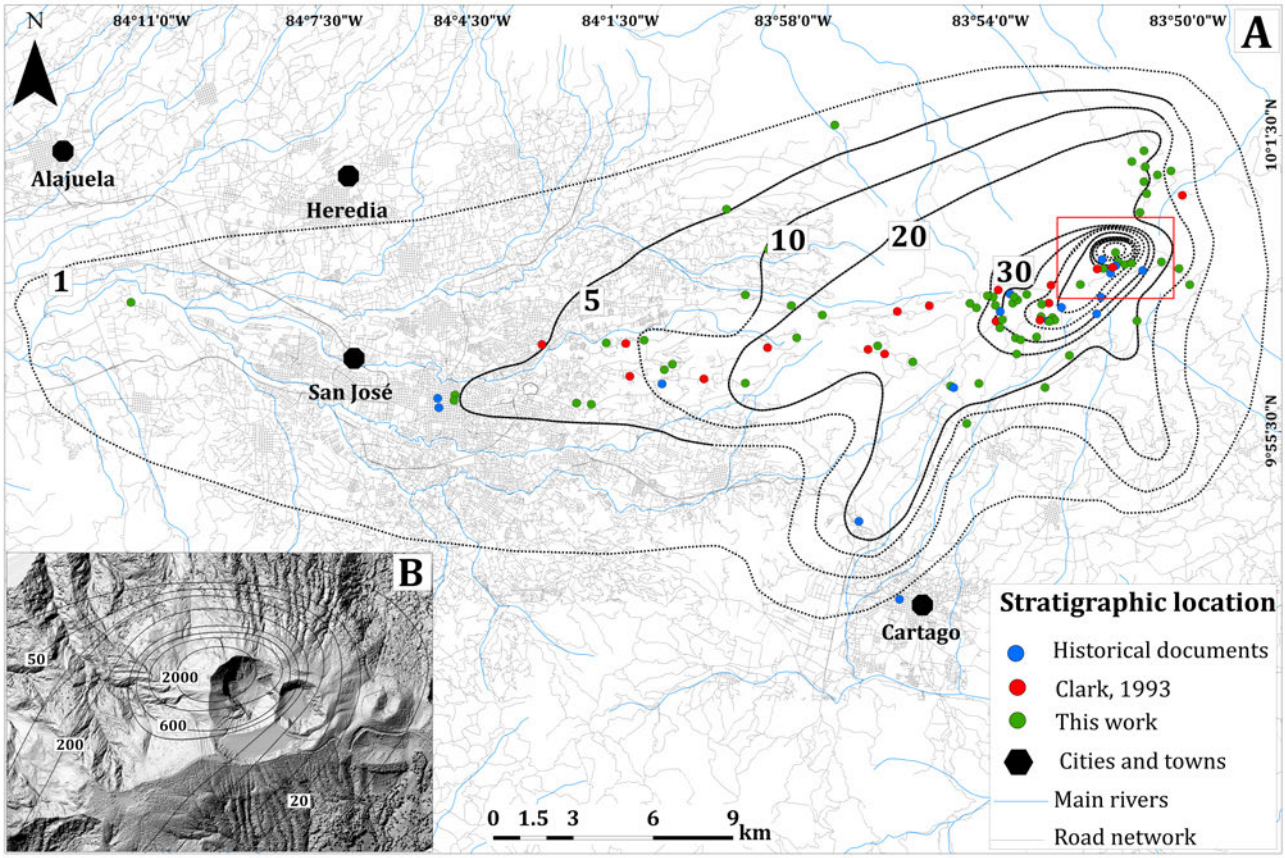

Figure 12: [A] Isopach map (cm) of the 1963–1965 eruption. [B] Inset of red box in (A) showing the thickness of the deposit in the proximal area. Due to scale constraints, some data points may appear superimposed.

commonly have sharp boundaries; however, some rounded or embayed grains also occur. Type 2 is texturally distinct, with clear cores bound by a dusty/cellular mantle that is overgrown by a clear zone. Crystal morphologies are commonly irregular, and twinned crystals traverse the entire grain in an optically continuous manner. The phenocrysts are mostly normally zoned (An_{78-50}), and rarely reverse (An_{56-70}). Complex zoning is rare; however, when present, crystals usually contain relatively sodic cores (An_{49-57}) with a compositional jump to a significantly more calcic (An_{58-70}) overgrowth rim. Orthopyroxene, which is generally subordinate to clinopyroxene, is weakly zoned (En_{70-78}). Augite rims around orthopyroxenes were also observed with regular contact. No differences were observed in the compositions of the composite crystals and isolated phenocrysts. The inclusion patterns (plag+mt) were similar to that present in clinopyroxene.

Several bombs contain small, partially resorbed lithic inclusions (<5 % modal; ≤0.1 mm up to 2.4 × 0.4 cm) that are angular to rounded or elongate. The inclusions are porphyritic with black to dark brown glass composed of abundant Fe-Ti oxide microlites and pyroxene crystallites. They are almost opaque in transmitted light and strongly resemble tachylite, but their composition is andesitic to dacitic.

Contact with the surrounding bomb is gradual (partially resorbed) to sharp with broken phenocrysts and vesicles at the boundary. Some tachylitic-like inclusions have open cracks that cross-cut phenocrysts. Furthermore, the tachylitic-like inclusions have subrounded vesicles (40–320 μm) smaller than the surrounding light brown groundmass of the host bomb, which has larger polymodal round vesicles (0.06–5.6 mm), and sometimes acicular crystals. In addition, in both the inclusions and bombs, some phenocrysts have a thin sideromelane-like rim (<60 μm of brown microlite-free andesitic to dacitic glass), surrounded by brown or dark glass or moderately microlite-rich groundmass, respectively. However, there was no significant difference in glass chemistry between the black and brown glasses, as would be expected, nor in phenocryst composition. SEM images of these layers indicate that the influence of external water was subordinate or absent, as the highly vesicular rock samples (Table 3, Figure 13) lack typical structures of magma-water interaction (i.e. planar and curviplanar surfaces, hydration and quenched cracks, chemical pitting; [**Heiken_1985**; Wohletz 1983]).

The geochemical variation of the juvenile components along the succession shows two main trends from base to top, with a marked compositional change occurring at sample ALGI 13b (Figures 7 and 14). This transition is clearly visible in the stratigraphic section and will be discussed in detail in the Discussion section.

Table 3: Representative microprobe glass analyses of the groundmass from the sample ALGI 6 (1963–1965 scoria). "Black" or "tachylitic" glass (BG) and "brown" or "sideromelane" glass (BwG) were analyzed.

ALGI 6	BG	BG	BG	BG	BwG	BwG	BwG
SiO_2	63.93	64.77	59.54	62.06	62.8	64.39	64.29
TiO_2	1.63	1.6	1.73	1.5	1.61	1.55	1.42
Al_2O_3	15.37	15.83	16.91	17.72	15.28	15.18	15.91
FeO_t	7.1	7.06	5.54	5.77	6.99	6.7	6.42
MnO	0.25	0.09	0.14	0.12	0.15	0.13	0.17
MgO	2.24	2.39	3.7	1.9	2.4	2.01	1.87
CaO	3.81	4.4	7.92	6.81	4.24	4.88	4.94
Na_2O	2.51	2.44	4.01	3.3	3.97	3.51	3.76
K_2O	3.68	3.35	2.03	2.24	4.51	3.29	3.13
Cr_2O_3	0.06	0.02	0	0	0.1	0	0.02
Total	100.58	101.95	101.52	101.42	102.05	101.64	101.93

5 Discussion

5.1 Interpretation of the tephra deposits

Murata et al. [1966] studied a 1.7 m thick section, deposited between March 1963 and June 23, 1964, accumulated just 800 m downwind of the vent. They interpreted many of the single layers as ashfall deposits; the origin of other rippled layers was interpreted at that time as the result of falling raindrops, sheet wash, and reworked eolian deposits. This locality is at the summit, approximately 280 m SW of our described section of RD (Figures 6 and 8). Murata et al. [1966] recognized also in June 1964, three "pumice"-rich layers that served as marker horizons in the ash sections to the west, southwest, and south of the vent. They suggest that these layers had formed during the period of mid-December 1963 through January 1964, when incandescent lava fountains occurred. The "pumice"-rich layers are still present in the RD sequence (Figure 5). The chemical analyses of these light-colored, scoriaceous, fine lapilli (referred to by Murata et al. [1966] as pumice) collected from the lower part of the RD with TiO_2 (<1.0 wt.%), P_2O_5 (<0.36 wt.%), K_2O (<2.1 wt.%), Ba (<810 ppm), Rb (<55 ppm), Sr (<805 ppm) and Zr (<190 ppm) correlated well with the first part of the stratigraphic section in the ICD based on the geochemistry of bombs. A pronounced chemical change (indicated with the letter P or sample code 13b) occurs in the stratigraphic succession of the ICD (Figures 6 and 14), with a first slight decrease in, and, from the middle of the section upwards with an enrichment in LILE (K, Rb, Sr, Ba, Zr, and Nb), P_2O_5, TiO_2, and Ce. This pattern is also recognized in the geochemical analyses from the RD (Figure 7), but those analyses were not plotted, because there are few samples compared to those taken in the ICD succession (Figures 6 and 14).

The second step was to correlate the isolated mud crack and accretionary lapilli layers in both ICD and RD as marker layers (Figures 6 and 7). The third step was to harmonize the narrative description of the four stages of volcanic activity (Figure 5), including the eruption styles and erosional stages (major unconformities) corresponding to the rainy seasons at that time with the interpretation of the observed facies in the preserved deposits. Using these methods, we can roughly estimate, and more accurately reconstruct, the depositional sequence of the major events in the stratigraphic columns, thus providing a synoptic evolution of the eruption.

Most eruptive deposits are fines-rich, finely bedded, poorly sorted and vesicular tuff layers, with abundant cohesive ash, accretionary lapilli, and large breadcrust blocks, penecontemporaneous deformation, and mud cracks. These features are typical of phreatomagmatic eruptions [**Lorenz_1974**; Fisher and Schmincke 1984]. Moreover, some deposits consist of bedded fine, brown ash deposited as wet cohesive material. Cracks appear as dilatational features in massive and consolidated wet beds. Most deposits are well-stratified ash deposits defined by laterally consistent planar bedding with internal laminations. They varied from moderately to well-sorted and alternate with massive ash-rich layers (Figures 7 and 10). The regular thickness of these beds indicates fallout.

The stratified ash layers show intercalated discontinuous lamination (ripples) and pinch-and-swell structures. They are relatively well sorted, thicken in depressions, and are consistently thinner with increasing distance from the crater rim (1–2 mm per meter of radial distance). These characteristics indicate lateral transport and deposition from intermittent dilute pyroclastic density currents (PDCs) also known as pyroclastic surges. The surge-like deposits are fine-grained and well-sorted, with a Gaussian distribution attesting to effective selection during transport in the tractional zone of the moving cloud. Some of the PDCs moved through falling tephra and ballistic blocks. Coarse-grained, massive, and laterally consistent planar bedding deposits related to sStages 1, 2, and 3, are consistent with fallout and dilute PDC structures. They can occur simultaneously because of their proximity to the crater, suggesting an emplacement following weakly explosive eruptions [**Cas_1989**]. Several dilute PDCs might have been deposited from currents fed by a collapsing eruption column or gravitationally segregated from the top of the concentrated PDCs.

The very thin, massive pyroclastic-rich layers, located primarily at the top of the ICD sequence (Stage 4, Figure 9), differ significantly from other recent intra-crater, post-eruptive, and resedimented unconsolidated pyroclastic deposits, which

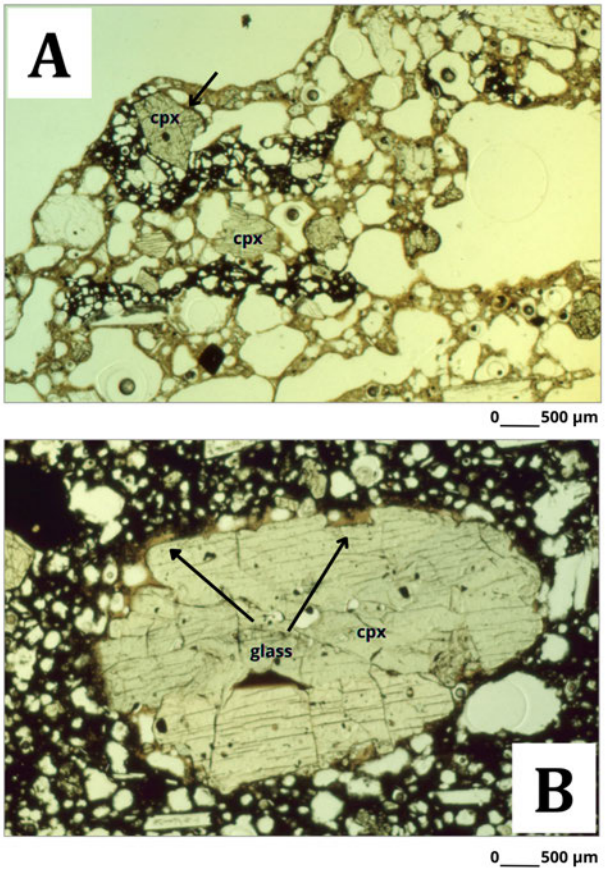

Figure 13: Vesicular juvenile bombs have two different groundmasses but similar mineralogical compositions. Note the difference in the size of the vesicles between the two groundmasses. [A] Elongate tachylitic-like inclusions (black) partially digested in interstitial groundmass. In the upper part, euhedral clinopyroxene (cpx) phenocrysts cut the contact between the two different groundmasses. [B] Cpx megacryst mantled by (light color) glass in a tachylitic-like inclusion (black on the left side) included in an interstitial groundmass.

commonly show meandering structures, reverse grading, or channel fillings [Solgevik et al. 2007]. However, there was no evidence of high-temperature emplacement (i.e. welding textures, degassing pipes, columnar jointed, thermal oxidation, charred woods), questioning the primary origin of these thin, massive beds. Four different mechanisms can be envisaged: (a) primary massive concentrated PDCs [cf. Cas and Wright 1987], (b) massive near-vent dilute PDCs [**Sohn_1989**], which is subject to debate [Valentine 1987; Valentine et al. 2017]; c) crystal-lithic-rich resedimented tephra deposits [cf. Cas and Wright 1987], and d) a variation of the previous one, as a remobilized tephra in a dry state by concentrated granular flows during or very shortly after eruption. This last mechanism requires slopes exceeding the angle of repose for tephra (~30–35°; [CARRIGY 1970]). At Irazú, the steep intra-crater slopes of the developing tuff cone (estimated at >25–30 °) and the irregular pre-existing crater morphology would have promoted instability and remobilization of freshly deposited, unconsolidated stratified deposits (interpreted as dilute PDC deposits), similar to processes documented at Ubehebe Crater in California, U.S.A. [Valentine et al. 2022].

All massive deposits (see Stage 4 in Figure 6) are relatively fine-grained and well- to poorly- sorted (1.35–2.2 ϕ). Grain-size characteristics and components of massive beds (e.g. samples Ira 1/30, Ira 2/4, and Ira 2/7) are similar to that of the thinly bedded ash/lapilli deposits (e.g. samples Ira 2/3 and Ira 2/6), but with a strong variation in thickness within short distances of meters. The coarse grain-size mode (between −4 and 0 ϕ) of the massive deposits in the upper ICD (sStages 3–-4) consists almost entirely of unaltered lithic fragments composed of basaltic andesite and older basaltic lavas, characterized by variably rounded to angular shapes. The angular clasts are interpreted as crater wall collapse material, derived from the progressive enlargement and deepening of the Active Crater during the eruption. In contrast, the rounded clasts likely represent recycled material that underwent abrasion during repeated ejection and fall back into the crater. The imbricate structure indicates that the flows were deposited from pyroclastic currents moving back toward the Active Crater because of the high slope and morphology of the western part of the crater. Usually, large clasts (bombs and blocks) do not show any signs of sag structures into underlying strata suggesting that they were deposited from a concentrated PDC.

The origin of the massive ash beds in the ICD is uncertain, with two competing interpretations. They may represent primary dense phreatomagmatic PDCs (ash-flow deposits) generated from low, collapsing eruption columns that were confined within the crater due to low kinetic energy and the barrier effect of crater walls. Alternatively, they may represent syn-eruptive dry granular flows formed by rapid remobilization of previously deposited stratified material (dilute PDC deposits) from the steep western crater wall (>25–30°), similar to processes documented at Ubehebe Crater [Valentine et al. 2020; 2022]. Distinguishing between these mechanisms is challenging because both can produce poorly sorted, massive to weakly stratified, fine-ash-rich beds. We favor the remobilization interpretation based on the analogy with Ubehebe Crater, the extremely steep intra-crater slopes that would promote instability, and the absence of features typical of sustained PDC transport (e.g. cross-stratification). However, primary low-energy PDC emplacement cannot be definitively ruled out, and a combination of both processes likely occurred.

There is only one thin bed of accretionary lapilli in both the ICD (7 cm thick) and RD (1.5 cm thick). This suggests that either the humidity in the environment near the crater was low and limited the formation of abundant accretionary lapilli, or that water vapor was superheated. The presence of tuffs (some vesiculated) plastered on upright tree trunks and in the Diego de la Haya crater wall or deposition against vertical surfaces as wall-paper-like bedded deposits indicates that deposition occurred in moist to wet conditions. The slumps could be related to wet deposits, but some were related to the rainy season.

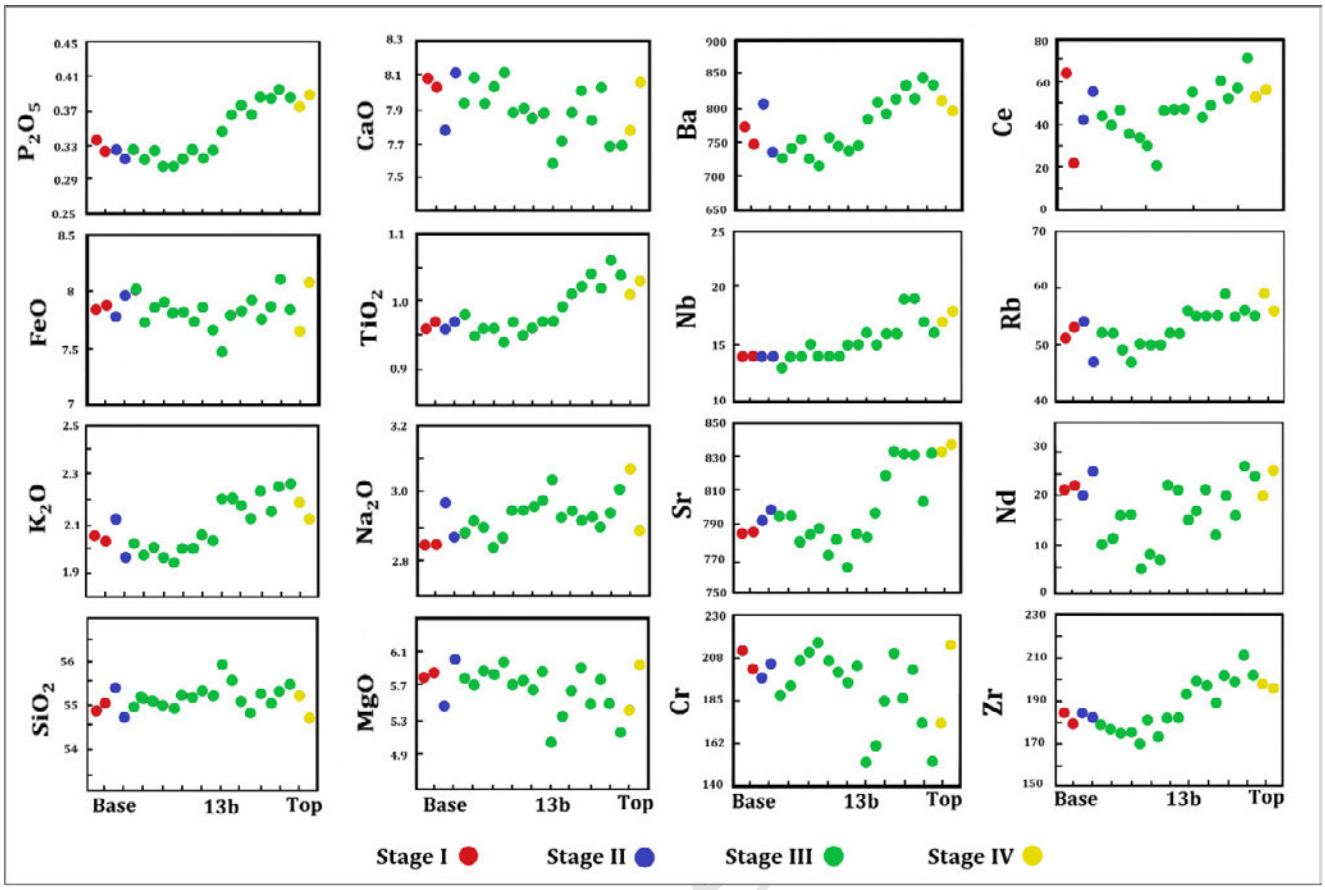

Figure 14: Changes in bulk rock major and trace elements with stratigraphic position at the intra-crater deposit (ICD). Rock sample 13b indicated the main geochemical change in the eruptive sequence (see also Figure 6 for details). The two columns on the left are given in wt.%, and the two columns on the right are given in ppm.

The well-sorted scoriaceous lapilli and bombs/juvenile blocks beds, with a few non-juvenile lithic clasts (<5%), in both ICD and RD could be emplaced by two potential mechanisms: fallout or ballistic curtain [Valentine et al. 2022]. In the RD the regular thickness of these scoria lapilli beds suggests a fallout origin. At the ICD, several of these layers are thicker and more abundant (at least 14 beds) in comparison with the RD (Table 1), where only thinner and less abundant layers (only 5 beds) are present in a short distance of less than 300 m, and a difference of elevation of about 90–100 m (see Table 1). The coarse-grained deposits at the ICD are not always well-sorted, and display a variable thickness in short distance, having an asymmetric Gaussian grain size distribution (e.g. samples Ira 2/3 and 2/5, Figure 6). The coexistence of spindle bombs and angular breadcrust bombs and lapilli suggests that some clasts remained fluid after fragmentation while others quenched early, which could indicate the existence of different active vents (some with a relatively cooled crust) in the Main Crater, as discussed in Section 2.1. Yellow brown, highly vesicular scoriae are minor, and the color difference between the two types of ejecta is due to differences in vesicularity and the degree of oxidation. Both types consist predominantly of moderate to highly vesicular juvenile bombs and lapilli.

Returning to the emplacement interpretation, particularly of the lapilli-bombs-block deposits, the strong differences between the number of layers and their thickness between the ICD and the RD suggest an asymmetric radial distribution of ballistic deposits. This preferential accumulation in the ICD is attributed to: (1) the pre-1963 intra-crater platform morphology (volcanic terrace) on the western crater wall, which provided a depositional surface for ballistic material; (2) the prevalent westerly wind direction, which deflected finer tephra toward the ICD; and (3) the lower elevation of the ICD (~90 m below the RD), which favored accumulation of ballistic clasts. These deposits are analogous to sheet-like deposits with variable thickness described for experimental ballistic curtains (i.e. eruption jets that collapse with simultaneous outward spreading; [**Graettinger_2015**]), like those interpreted in maar volcanoes favored by a relatively flat terrain that produce the widest spread and extend of ballistic curtain deposits [**Valentine_2015b**; Ort et al. 2018; Valentine et al. 2022]. Historical near-field photographs and videos (50 to 450 m of distance from the crater rim), all taken from the SSE side of the Active Crater, suggested that the trajectory of the ballistic was parabolic as an umbrella, but also as inclined jets (Figure 15). Isolated ballistic bombs and blocks that produced sag structures in finer-grained deposits are common in both ICD and RD. Most of these scoriaceous deposits (highly vesic-

ular bombs/lapilli) are interpreted as products of Strombolian eruptions.

The occurrence of hydrothermally altered and unaltered lithics (diameter ≤20 cm) immersed in brown ash with sag structures and the lack of evident juvenile clasts are inferred to be phreatic deposits. One example of this type of deposition occurred on August 26, 1964, when "*jets of yellowish muddy water shot out of the vent to heights of 25–30 meters above the level of Playa Hermosa and landed on the Playa...*" [Murata et al. 1966]. These breccias could also represent ballistic curtains that form when discrete eruptive jets collapse and expand radially, thereby generating poorly sorted tuff breccias [Valentine et al. 2017].

The role of preexisting craters is very important in the ejecta distribution (laterally or vertically directed) and the different depths of the explosions as it was discussed by **Valentine_2015a**. In fact, prior to the 1963 eruption, the crater of Irazú was populated by several small pit craters (Figure 8), which were gradually engulfed by the growth of the Active Crater during the eruptive activity that began in 1963. The previous eruptive foci, coupled with the existence of two or three active vents (mentioned ~~pages before~~ in Section 2.1) at the bottom of the Irazú crater during the eruptive climax, could have conditioned the direction of some inclined eruptions as jets of ballistic blocks and fluid mud waters.

5.2 Physical volcanology of the tephra sequence

The stratigraphy of the 1963–1965 deposits is complex and reflects the changes in activity during the four eruptive stages described above. Based on the phenocryst fraction (27.6–33.6 %) and frequent Strombolian explosions (Figure 3), we infer a relatively lower viscosity during the first two stages of the eruption (i.e. January 1963 to January 1964), compared to later stages (35.0–39.7 %). The increasing viscosity of the magma probably contributed to more efficient fragmentation, resulting in fine-grained deposits (i.e. dense phreatomagmatic PDCs) in the later stages, as observed in other eruptions [e.g. Dingwell 1998; Patrick et al. 2007].

Several features of the 1963–1965 tephra sequence support nearly continuous phreatomagmatism as a dominant fragmentation mechanism, although sporadic Strombolian and phreatic events were also present in the earlier stages. Two types of phreatomagmatic eruptions occurred during the 1963–1965 eruption. One type was a weak, near-continuous, gas and ash emission with convective column heights generally ~0.5 km. The other style consisted of large discrete explosions accompanied by tephra jets and large convective clouds of ash and steam columns several kilometers in height (1 to 8, even 11 km). The eruptions, in general, were characterized by the explosive ejection of bombs and juvenile blocks, which were commonly incandescent at the vent but too viscous to become rounded during flight (Figure 14). The description of activity during several stages of the eruptive period indicates that "*strong, reverberant explosions*" [Murata et al. 1966] were typically associated with "*trembling of the ground*," and steam eruptions were accompanied by ash. On August 26, 1964, major rainfall and "*sharp earthquakes*" (different from earlier tremor) were associated with water-jets (phreatic eruptions). This type of earthquake occurred on August 30, 1964. Therefore, the 1963–1965 eruption was thermally heterogeneous because it ejected both incandescent clasts and liquid water.

The hydrogeology [**Alvarado_1993**; **Ulloa_2018**] indicates that the volcanic conduit could intersect three different shallow aquifers at different levels. In hand samples and SEM images, the juvenile particles show a wide spectrum of texture, from vesicular bombs (due to the exsolution of magmatic gases) to high-density and chilled juvenile bombs. In fact, the small pyroclasts (<1 mm diameter) are vesicular with irregular to smooth fluidal shapes. This morphology suggests significant vesiculation of the magma prior to explosive interaction with external water [**Heiken_1985**].

The lithics were mainly derived from a hydrothermally altered portion of the volcano, perhaps located below the shallow aquifer, which briefly interacted with magma during several stages of the eruption. However, some of the lithics (hydrothermally altered) were also present in the older deposits present in the vent that were eroded during the eruptions (Figure 16).

Fluctuations in the influx rates of magma and external water at Irazú have resulted in complex patterns of wet and dry eruptions. Therefore, if magma flux temporarily increases during some phases of the eruption, it might overwhelm the effects of magma/water interactions, leading to normal degassing and vesiculation that produced Strombolian eruptive styles [Aravena et al. 2018]. Observations of incandescence and glowing lava suggest that the magma was relatively close to the surface between December 1963 and January 1964, indicating that the rise of new magma exceeded the discharge rate during the previous Strombolian phase. Another reason could be that one of the several vents, particularly those located in the center, could have intruded a section lacking an aquifer.

However, in a tropical country like Costa Rica, where rainy and dry seasons are well defined, seasonal variations significantly affect aquifer recharge. The water table rises during the rainy season (late May or June to November or mid-December) and drops notably during the dry season (mid-December to May) due to the lack of precipitation [**Alpzar_2016**; **Macas_2016**; **Gonzlez_2023**]. In addition, during El Niño conditions, rainfall is substantially reduced by up to 69.2 %, limiting groundwater recharge. In contrast, La Niña is associated with increased rainfall during the rainy season, and groundwater recharge can increase by up to 94.7 % during active cold front periods [**Snchez-Murillo_2022**; **Snchez-Murillo_2023**]. Clearly, this will depend on the recharge area, the permeability of the surrounding volcanic medium, and whether the aquifer is confined or unconfined, which will be reflected in water table levels sooner or later. Notably, moderate El Niño conditions were present in Costa Rica (with reduced rainfall) during 1963, whereas La Niña conditions prevailed in 1964 [**Len_2020**; Huang et al. 2017], and the eruptive period ended in early 1965. In the case of Irazú, the recharge areas for the three shallowest unconfined aquifers are small (Figure 16), so during the dry season, aquifer levels should drop notably.

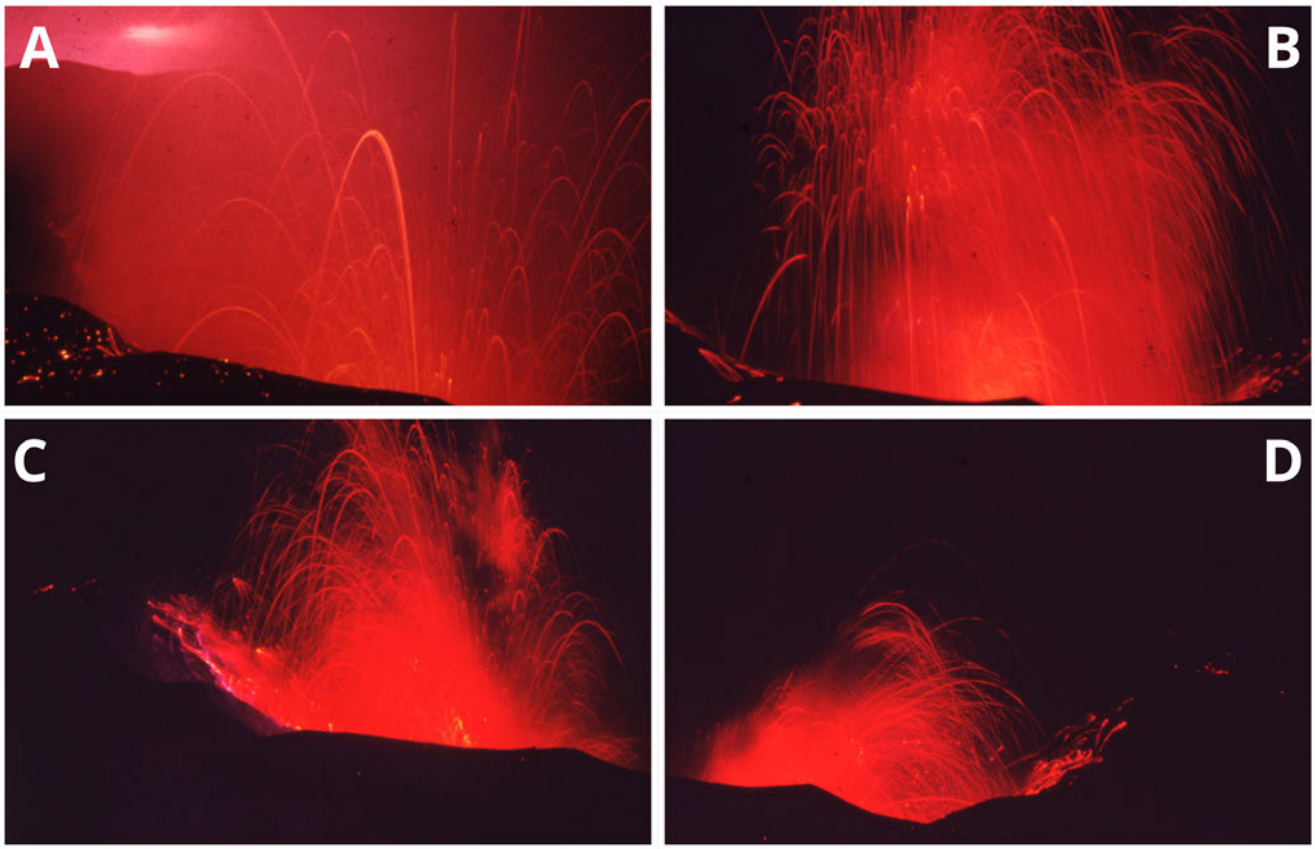

Figure 15: Typical ejection patterns of glowing bombs in late 1963 or early 1964. [A]–[B] Parabolic trajectories. [C] High-angle ballistic trajectory. [D] More low-angle and appearing to be derived from two different foci. Images courtesy of Walter Shäer, R.I.P.

If we pay attention to the stratigraphic column and its chronological correlation (Figures 6 and 7), most of the magmatic deposits are present in periods corresponding to the dry season at Irazú (mid-December to early May), which could be interpreted as the result of groundwater depletion in the local aquifers, thereby inhibiting magma-water interaction. In addition, during most of the eruptive period in 1964, La Niña conditions were present, favoring greater groundwater recharge, which could be reflected in a higher probability of phreatomagmatic eruptions during the rainy season—even at the beginning of 1965—because aquifer levels do not drop immediately with the onset of the dry season.

The rapid onset of Strombolian and phreatomagmatic ballistic jets increased in intensity following seismic shocks (e.g. July 17 and December 1963; June 7, 1964), which could relate to the rainy season, but also the heavy rain on December 9–10 of 1963 in which the aquifers were saturated. In addition, the role of seismic earthquakes can promote the formation and propagation of fractures to favor magma-water interaction phreatomagmatic fragmentation [cf. Wohletz 1983; Zimanowski et al. 1991]. It seems likely that the magma flux was relatively slow during most parts of the eruption, although it is difficult to infer from the evidence [see Valentine et al. 2017]. There are several examples in literature where eruptions shifted between magmatic to phreatomagmatic, but few historical cases related to maar formation [e.g. White and Ross 2011; Valentine et al. 2017; Ort et al. 2018].

It is uncertain whether the dilute PDCs found on the Playa Hermosa Plain were emplaced at a high flow velocity and temperature. However, visitors and tourists were often present on the rim of the Active Crater day and night and in areas where dilute PDCs deposits were recognized, because the Irazú eruption was a tourist attraction without any safety regulations (see Figure 3). During the course of the eruption, only two people were killed by ballistic blocks, although several were reported to have been injured by "debris and acid burns near the crater". Thus, a directional and moderate- to low-temperature ash cloud described in the newspaper *La República* on April 14, 1964, could represent a dilute PDC. Several dilute PDC deposits in the RD have current markers pointing in both directions, suggesting that many deposits experienced ash-cloud convective currents that drove back into the crater. The non-charred, still-standing trees plastered by dilute PDC deposits also suggest a relatively low- to moderate-energy movement and low- to moderate-temperature emplacement. The absence of megaripples and long wavelengths in the sand-wave structures supports a lower energy transport mechanism. Although possibly speculative, several photographs and movies of the eruption support the idea of low temperature and low velocity of the dilute PDCs. Thus, the dilute PDCs at Irazú could represent the elutriation from the top of a moving, very

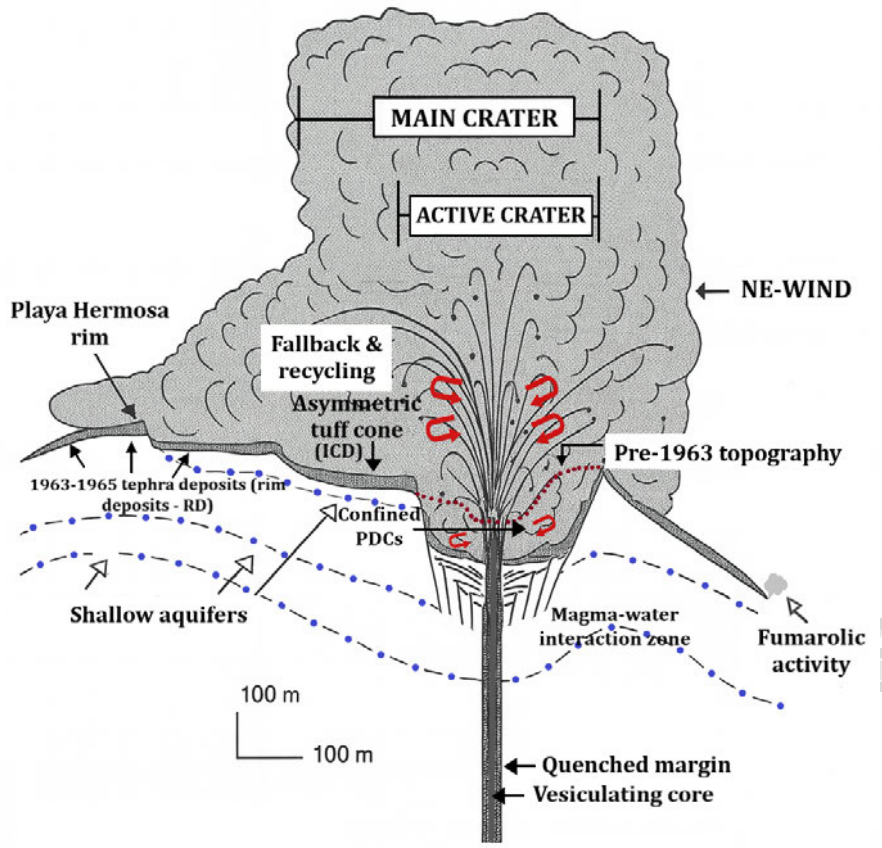

Figure 16: Schematic section of the summit of Irazú and the model of typical activity (see text for details). The zone of circulating water (blue dots and dashed black lines) represents different aquifers. The dotted red line indicates the pre-1963 rim of Active Crater. During a typical eruptive phase, strong winds preferentially disperse the tephra, generating an asymmetric tuff cone that grows and overhangs plastering into the volcanic terrace and crater rims. Pyroclastic density currents (PDCs), slides, water-rich tephra deposits (slurry), and penecontemporaneous slumping generated flow back into both, the Active Crater (red thick curved arrows) and the Main Crater forming hybrid deposits within the proximal region of the tuff ring and favoring the recycling of tephra.

concentrated PDC, by partial asymmetric collapse of the ash plume [see Carey et al. 1988], which was strongly directed by moderate winds up to 43.5 km h^{-1} [**Coen_1964**] and modified by traction-controlled deceleration due to topography.

5.3 Crater growth, vent geometry and tephra recycling

Before 1963, the crater dimensions were small, and they grew significantly in size (diameter and depth) during the eruption. The best estimate of the crater growth volume is approximately $25 \pm 3 \times 10^6$ m^3. This suggests that the crater should have grown dominantly by subsidence and collapse of slump blocks, like maar-like craters (i.e. collapse rim crater and vent filled by volcanic debris and breccias), in addition to PDCs deposits and rim-tuff formation [**Valentine_2015a**; Lorenz 1986], although maar craters are usually cut into a flat pre-eruption land surface with their floor lying below the pre-eruptive surface [Lorenz 1986; White and Ross 2011], which is not the case of Irazú volcano. The crater developed an asymmetric tuff cone on the western side, in which dilute PDC deposits are more abundant, as also described for other tuff rings and even in maars [**Valentine_2015b**; cf. Wohletz 1983; White and Ross 2011; Valentine et al. 2022]. The final crater shape of Irazú could depend on the location of previous pit craters (as was previously described in Irazú by **Elizondo_2019**) and the location of foci epicenters at the moment of the eruption as predicted by empirical experiments [**Valentine_2015a**].

During the explosive activity, coarse material fell back into the large crater to undergo further abrasion and fragmentation, basically "*the volcano functioning as a veritable rock crusher and dust-machine*" [cf. Murata et al. 1966]. After each collapse and fragmentation, more water was vaporized, and the cycle was repeated. This was the case for the explosive episodes on July 3, 1963. The previously asymmetric funnel-shaped topography on the western side favored this process. In fact, the ICD in that area has several indicators of lateral transport though the crater, such as soft-state folding and the imbrication of clasts, among other sheet flow sedimentary structures. Strong thickening of tephra deposits and their ramping up tree trunks on the side opposite to the crater indicate that some dilute PDCs impacted the Playa Hermosa crater wall and were deflected downwards. The lithic component of the deposits includes pre-existing pyroclastic rocks fragmented during earlier explosive activity, and hydrothermally altered material derived from crater wall erosion. These materials, together with sheet erosion and slumping of proximal tephra, contributed to the recycled component that fell back into the crater.

As described in the petrographic section, several bombs have small angular to rounded or elongate porphyritic tachylyte-like inclusions that are partially resorbed (Figure 13). The acicular crystals and the large proportion of light brown glass in the brown groundmass of the bombs suggest rapid cooling, but the wide range in vesicle size suggests that vesiculation continued immediately after or during the eruption. In addition, in both the inclusions and bombs, some phenocrysts have a thin sideromelane-like rim surrounded by tachylitic-like or moderately microlite-rich groundmass, respectively. This implies that some of these inclusions were in a solid state

before they were included in the bomb, whereas others were still plastic (Figure 13).

The more developed phreatomagmatic deposits and changes in the abundance of ash upward through the ICD (Stage 4, Figure 9) suggest an increase in the water/magma ratio as the eruption progressed, as well as tephra recycling because of a greater efficiency in the degree of fragmentation. Dissolution pits (not included in Figure 11) on the surface of several ash grains are features typically observed in recycled ash [Deardorff and Cashman 2017].

Application of Sequential Fragmentation and Transport theory (SFT) to the 1963–1965 Irazú proximal tephra revealed that the grain size of sub-population modes decreased over time, suggesting a progressively greater degree of recycling [**Brenes_2013**]. This grain-size reduction is attributed to abrasive processes—repeated fragmentation, inter-clast collisions, and mechanical wear—that intensified as tephra accumulated and was repeatedly recycled within the crater. Additionally, the progressive deepening of the crater floor (increasing scaled depth of explosions) reduced the distances at which coarse material could be ejected [Valentine et al. 2017], further promoting the retention and recycling of larger clasts within the crater.

The textural evidence for recycling observed in clasts include changes in morphology, color and luster, precipitation of sublimates on external surfaces, varying degrees of matrix crystallinity and deformation, and an oxide-rich layer surrounding the included clasts [**Alvarado_1993**; **DOriano_2014**; Houghton and Smith 1993; Deardorff and Cashman 2017]. The existence of different vents in the Main Crater with fresh exposed crust of lava also provide a mechanism to explain, in part, the differences among clasts, ranging from highly vesicular bombs, poorly vesicular bombs, and non-vesicular juvenile blocks, as is the case for other volcanoes [e.g. Houghton and Hackett 1984; Houghton and Schmincke 1986; Houghton and Wilson 1989]. Thus, the juvenile tephra represents a mixture of (a) newly arrived, bubble-rich magma from one or multiple vents of contrasting styles, (b) magma that had undergone significant bubble coalescence and partial degassing during a repose period in the vent, such as lava ponding, (c) pyroclasts that fell back into the crater, (d) fragments of quenched magma along the vent walls, and (e) magma mixing entrainment of partly solidified and evolved magma batches at depth.

The increasing abundance of lithics (both fresh and hydrothermally altered) in the upper half of the ICD stratigraphic sequence (Stage 4) indicates that the vent had become larger and was more thoroughly cleared compared to the first few months of the eruption (January 1963 to May 1964). The crystals present in the PDCs have both rounded and angular shapes, partly because they were previously corroded by magmatic processes, but principally because of abrasion and recycling.

5.4 5.4 General petrological interpretation

Ruprecht and Plank [2013] and Oeser et al. [2018] showed a wider range of chemistry in the olivines analyzed ($Fo_{71.5–91.5}$). Thus, chemically, it is possible to distinguish and interpret three populations: (a) a primitive and deep MgO-rich olivine xenocryst (~30 km), rich in Ni ($Fo_{89–91}$), (b) complex olivine xenocrysts with significant reverse zonation (core $Fo_{80–87}$ and rim $Fo_{87–90}$), also reflected in Ni, P, and Cr content at intermediate depths (>15 km), and (c) olivine with intermediate to low Fo content and normal zoning (core Fo_{80-90} and rim $Fo_{70–84}$), and low Ni content reflecting more superficial processes of fractionation and mixing conditions (<10 km). This suggests a deep magmatic source with a series of more superficial mixing and crystal fractionation processes, including several magma batches in the upper crust and even within the volcanic edifice itself, as supported by seismological, thermobarometric, and crustal deformation data [**Alvarado_2006**; Muller et al. 2024].

The rock and mineral compositions provide the most compelling evidence that magma mixing and recharge triggered the eruption. In particular, the complex zoning patterns shown by the clinopyroxene and plagioclase phenocrysts in basaltic andesite are difficult to reconcile with a simple, isobaric, fractional crystallization model. The two populations of plagioclases with different geochemical signatures and zonation suggest mixing, because it is the only mechanism that accounts for bimodal composition populations in any single phenocryst phase in a rock sample [**Glazner_1990**]. Pyroxene data also suggested two populations of clinopyroxenes. Magnesium-rich pyroxenes and olivines indicate the presence of mafic recharge magma [**Alvarado_2006**; Ruprecht and Plank 2013]. Clinopyroxene rims around orthopyroxene, apatite and melt inclusions may have resulted from the mixing of 69 % Cl-rich [**Boyce_2009**] but clinopyroxene-undersaturated basaltic andesite and 32 % clinopyroxene-saturated MgO-rich basalt [**Alvarado_2006**]. Trace element and isotopic zoning in olivines suggest that recharge magmas that triggered the 1963–1965 eruption traveled from the Moho to the surface within months to a year [Ruprecht and Plank 2013; Oeser et al. 2018]. The preservation of heterogeneous populations of apatite and internally heterogeneous crystals also requires short timescales (days to months) for these magmatic processes to occur [**Boyce_2009**]. Additional evidence for disequilibrium is provided by the distinctive composition of the 1963–1965 magma, which shows high concentrations of incompatible elements as well as Cr and Ni. The high values of Ni (75–107 ppm, average 94 ppm) and Cr (150–212 ppm, average 190 ppm) in the 1963–1965 magma preclude an origin by crystal fractionation involving mainly olivine, which is rare for basaltic andesites or andesites at Irazú but common for basalts.

The pronounced chemical change—first a slight decrease in incompatible elements (sStages 1, 2, and early Stage 3; Figure 13), followed by marked enrichment in LILE (K, Rb, Sr, Ba), HFSE (Zr, Th), P_2O_5, TiO_2, and Ce (late Stage 3 and Stage 4)—can be interpreted as evidence for a new injection of basaltic andesitic magma. This compositional shift likely occurred during the first half of 1964 (approximately June 1964), coinciding with the transition from Stage 2 to Stage 3 eruptive activity. This interpretation is consistent with petrographic evidence of magma mixing, including reversely zoned plagio-

clase, magnesian olivine ($Fo_{87–91}$), and disequilibrium mineral assemblages.

The inferred magma recharge correlates with observed changes in eruptive behavior: Stage 3 was characterized by intensified explosive activity, increased eruption column heights, and a shift toward more sustained phreatomagmatic explosions compared to the earlier stages. Apparently, two things were happening at the same time: La Niña was increasing the water present in the aquifers, favoring magma-water interaction, and the recharge was increasing the magma flux.

6 Conclusions

The most recent eruption at Irazú volcano between 1963 and 1965 and its deposits, although frequently cited in the literature, has not been previously studied in detail. The 1963–1965 eruption of Irazú is unusual because it resembled the development of a phreatomagmatic maar-like crater surrounded by a tuff ring, although it occurred at the summit of an andesite shield volcano. The eruption was predominantly phreatomagmatic, with subordinate Strombolian and rare phreatic events, producing ~6.2×10^7 m^3 of tephra (DRE: 5.68×10^7 m^3; VEI 3) over 25 months. Four eruptive stages were identified by correlating the ~28 m thick intra-crater deposits (ICD) and ~5.7 m thick rim deposits (RD) with contemporary observations. The deposits include fallout beds, ballistic curtain deposits, dilute PDC deposits, and massive ash beds interpreted as syn-eruptive dry granular flows remobilized from steep crater slopes.

Several factors conditioned the lateral and vertical facies extent of the tephra deposits, as well as their granulometry and fabric: (a) the irregular morphology of the western part of the Active Crater (volcanic terrace), (b) the previous small pit craters and the location of new foci on the floor of the Active Crater, (c) the enlargement of the crater in diameter and depth intersecting aquifers, (d) the westerly wind direction, (e) rate of magma flux, and (f) degree of aquifer recharge. The degree of aquifer recharge is controlled not only by seasonal rainfall patterns (dry vs. rainy season) but also by the El Niño–La Niña cycle. Given that groundwater levels may influence eruptive style, these climatic variations—including El Niño (drier conditions) and La Niña (wetter conditions)—may have affected the character of the eruption.

The steep, funnel-shaped crater geometry played a critical role in controlling depositional processes. Importantly, crater wall confinement prevented dilute PDCs from escaping beyond the crater rim, effectively redirecting flows back toward the vent area. This confinement mechanism not only enhanced tephra recycling and clast abrasion within the crater but also "protected" the outer slopes from potentially damaging gravity-fed PDCs. This represents a previously underappreciated process in summit crater eruptions that may have significant implications for hazard assessment.

The recognition of extensive tephra recycling—evidenced by abraded clast surfaces, progressively finer grain sizes through time, and mixed juvenile-recycled populations—demonstrates that crater-confined, long-duration eruptions can function as natural "rock crushers," systematically processing and refining tephra through repeated ejection-fallback cycles. This has important implications for interpreting grain-size distributions and volume estimates in similar settings.

The 1963–1965 eruption demonstrates that even moderate-intensity summit eruptions (VEI 3) at Irazú can sustain prolonged activity affecting the densely populated Greater Metropolitan Area of Costa Rica. Future eruptions may exhibit similar crater-confined dynamics, with: (1) asymmetric tephra distribution controlled by wind and crater morphology, (2) potential for syn-eruptive remobilization generating localized granular flows, (3) enhanced recycling producing fine ash that can disperse over greater distances, and (4) progressive crater enlargement increasing the potential for larger-scale collapses.

The processes documented at Irazú—crater-confined PDCs, tephra recycling, and maar-like development at a summit crater—are likely applicable to other volcanoes with similar geometries and phreatomagmatic activity. The detailed stratigraphic and sedimentological framework presented here provides a template for interpreting complex proximal deposits at these systems. New XRF analyses reveal a compositional shift around June 1964, with enrichment in incompatible elements indicating magma recharge that correlates with intensified Stage 3–4 activity. This demonstrates that geochemical monitoring of tephra can provide insights into subsurface magmatic processes during ongoing eruptions.

Author Contributions

Please provide author contribution statement

Acknowledgements

The field and laboratory work were funded by the Deutscher Akademischer Austauschdienst (DAAD), Instituto Costarricense de Electricidad (ICE) to GEA, and by the Deutsche Forschungsgemeinschaft (DFG) Leibniz grant between 1990–1993. We thank L. La Volpe, S. Chiesa, G. Civelli, P.F. Dellino, C. Schirnick, G.J. Soto, and J.F. Arias for their cooperation, helpful suggestions, and critical comments on the early manuscript draft. T. Solamacchia, J. Viramonte, H. Murcia, D. Szymanski, and P. Ruprecht have also provided valuable comments. A recent field trip in 2020 was supported by the Comisión Nacional de Prevención de Riesgos y Atención de Emergencias. More recently, G. Valentine and C. D'Oriano provided careful reviews and suggestions that improved and sharpened the manuscript significantly, in a way and with patience that is difficult to thank properly. The editor A. Hornby gives us a new opportunity to present a better version of the present paper, but he also contributed enormously with valuable observations. We thank P. C. Ryan and B. Hosseini for their careful review of the manuscript and for their improvements to the English language. We regret that H.-U. Schmincke could not see the final result of the study he inspired.

Data Availability

Please provide data availability statement.

Copyright Notice

References

Aravena, A., M. d. M. Vitturi, R. Cioni, and A. Neri (2018). "Physical constraints for effective magma-water interaction along volcanic conduits during silicic explosive eruptions". *Geology* 46(10), pages 867–870. DOI: 10.1130/g45065.1.

Carey, S. N., H. Sigurdsson, and R. S. J. Sparks (1988). "Experimental studies of particle-laden plumes". *Journal of Geophysical Research: Solid Earth* 93(B12), pages 15314–15328. DOI: 10.1029/jb093ib12p15314.

CARRIGY, M. A. (1970). "Experiments on the angles of repose of granular materials". *Sedimentology* 14(3-4), pages 147–158. DOI: 10.1111/j.1365-3091.1970.tb00189.x.

Cas, R. A. F. and J. V. Wright (1987). *Volcanic Successions Modern and Ancient*. Springer Netherlands. ISBN: 9789400931671. DOI: 10.1007/978-94-009-3167-1.

Deardorff, N. and K. Cashman (2017). "Rapid crystallization during recycling of basaltic andesite tephra: timescales determined by reheating experiments". *Scientific Reports* 7(1). DOI: 10.1038/srep46364.

Dingwell, D. B. (1998). "Recent experimental progress in the physical description of silicic magma relevant to explosive volcanism". *Geological Society, London, Special Publications* 145(1), pages 9–26. DOI: 10.1144/gsl.sp.1996.145.01.02.

Fisher, R. V. and H.-U. Schmincke (1984). *Pyroclastic Rocks*. Springer Berlin Heidelberg. ISBN: 9783642748646. DOI: 10.1007/978-3-642-74864-6.

Houghton, B. F. and R. T. Smith (1993). "Recycling of magmatic clasts during explosive eruptions: estimating the true juvenile content of phreatomagmatic volcanic deposits". *Bulletin of Volcanology* 55(6), pages 414–420. DOI: 10.1007/bf00302001.

Houghton, B. F. and C. J. N. Wilson (1989). "A vesicularity index for pyroclastic deposits". *Bulletin of Volcanology* 51(6), pages 451–462. DOI: 10.1007/bf01078811.

Houghton, B. and W. Hackett (1984). "Strombolian and phreatomagmatic deposits of Ohakune craters, Ruapehu, New Zealand: A complex interaction between external water and rising basaltic magma". *Journal of Volcanology and Geothermal Research* 21(3-4), pages 207–231. DOI: 10.1016/0377-0273(84)90023-4.

Houghton, B. and H.-U. Schmincke (1986). "Mixed deposits of simultaneous strombolian and phreatomagmatic volcanism: Rothenberg volcano, east Eifel volcanic field". *Journal of Volcanology and Geothermal Research* 30(1-2), pages 117–130. DOI: 10.1016/0377-0273(86)90069-7.

Huang, B., P. W. Thorne, V. F. Banzon, T. Boyer, G. Chepurin, J. H. Lawrimore, M. J. Menne, T. M. Smith, R. S. Vose, and H.-M. Zhang (2017). "Extended Reconstructed Sea Surface Temperature, Version 5 (ERSSTv5): Upgrades, Validations, and Intercomparisons". *Journal of Climate* 30(20), pages 8179–8205. DOI: 10.1175/jcli-d-16-0836.1.

Kruse, S., R. Mora-Amador, C. Ramírez, and G. E. Alvarado (2010). "Imágenes con el radar de penetración terrestre en la tefroestratigrafía reciente de los volcanes Poás e Irazú, Costa Rica". *Revista Geológica de América Central* (43). DOI: 10.15517/rgac.v0i43.3460.

Krushensky, R. D. and G. Escalante (1967). "Activity of Irazú and poás volcanoes, Costa Rica, November 1964 – July 1965". *Bulletin Volcanologique* 31(1), pages 75–84. DOI: 10.1007/bf02597006.

Lorenz, V. (1986). "On the growth of maars and diatremes and its relevance to the formation of tuff rings". *Bulletin of Volcanology* 48(5), pages 265–274. DOI: 10.1007/bf01081755.

Muller, C., G. E. Alvarado, M. Angarita, and G. Avard (2024). "Spatiotemporal deformation and activity distribution of Irazú and Turrialba volcanoes, Costa Rica: Are these volcanoes interconnected?" *Journal of Volcanology and Geothermal Research* 449, page 108052. DOI: 10.1016/j.jvolgeores.2024.108052.

Murata, K. J., C. Dondoli, and R. Saenz (1966). "The 1963–65 eruption of Irazú volcano, Costa Rica (the period of March 1963 to October 1964)". *Bulletin Volcanologique* 29(1), pages 763–793. DOI: 10.1007/bf02597194.

Oeser, M., P. Ruprecht, and S. Weyer (2018). "Combined Fe-Mg chemical and isotopic zoning in olivine constraining magma mixing-to-eruption timescales for the continental arc volcano Irazú (Costa Rica) and Cr diffusion in olivine". *American Mineralogist* 103(4), pages 582–599. DOI: 10.2138/am-2018-6258.

Ort, M. H., N. S. Lefebvre, C. A. Neal, V. S. McConnell, and K. H. Wohletz (2018). "Linking the Ukinrek 1977 maar-eruption observations to the tephra deposits: New insights into maar depositional processes". *Journal of Volcanology and Geothermal Research* 360, pages 36–60. DOI: 10.1016/j.jvolgeores.2018.07.005.

Patrick, M. R., A. J. L. Harris, M. Ripepe, J. Dehn, D. A. Rothery, and S. Calvari (2007). "Strombolian explosive styles and source conditions: insights from thermal (FLIR) video". *Bulletin of Volcanology* 69(7), pages 769–784. DOI: 10.1007/s00445-006-0107-0.

Ruprecht, P. and T. Plank (2013). "Feeding andesitic eruptions with a high-speed connection from the mantle". *Nature* 500(7460), pages 68–72. DOI: 10.1038/nature12342.

Sheridan, M. F. and K. H. Wohletz (1983). "Hydrovolcanism: Basic considerations and review". *Journal of Volcanology and Geothermal Research* 17(1-4), pages 1–29. DOI: 10.1016/0377-0273(83)90060-4.

Solgevik, H., H. B. Mattsson, and O. Hermelin (2007). "Growth of an emergent tuff cone: Fragmentation and depositional processes recorded in the Capelas tuff cone, São Miguel, Azores". *Journal of Volcanology and Geothermal Research* 159(1-3), pages 246–266. DOI: 10.1016/j.jvolgeores.2006.06.020.

Valentine, G. A. (1987). "Stratified flow in pyroclastic surges". *Bulletin of Volcanology* 49(4), pages 616–630. DOI: 10.1007/bf01079967.

Valentine, G. A., J. Fierstein, and J. D. White (2020). "Soft sediment deformation in dry pyroclastic deposits at Ubehebe Crater, Death Valley, California". *Geology* 49(2), pages 211–215. DOI: 10.1130/g48147.1.

– (2022). "Pyroclastic deposits of Ubehebe Crater, Death Valley, California, USA: Ballistics, pyroclastic surges, and dry granular flows". *Geosphere* 18(6), pages 1926–1957. DOI: 10.1130/ges02526.1.

Valentine, G. A., J. D. L. White, P.-S. Ross, A. H. Graettinger, and I. Sonder (2017). "Updates to Concepts on Phreatomagmatic Maar-Diatremes and Their Pyroclastic Deposits". *Frontiers in Earth Science* 5. DOI: 10.3389/feart.2017.00068.

Walker, G. P. L. (1973). "Explosive volcanic eruptions — a new classification scheme". *Geologische Rundschau* 62(2), pages 431–446. DOI: 10.1007/bf01840108.

– (1981). "Generation and dispersal of fine ash and dust by volcanic eruptions". *Journal of Volcanology and Geothermal Research* 11(1), pages 81–92. DOI: 10.1016/0377-0273(81)90077-9.

White, J. and P.-S. Ross (2011). "Maar-diatreme volcanoes: A review". *Journal of Volcanology and Geothermal Research* 201(1-4), pages 1–29. DOI: 10.1016/j.jvolgeores.2011.01.010.

Wohletz, K. H. (1983). "Mechanisms of hydrovolcanic pyroclast formation: Grain-size, scanning electron microscopy, and experimental studies". *Journal of Volcanology and Geothermal Research* 17(1-4), pages 31–63. DOI: 10.1016/0377-0273(83)90061-6.

Zimanowski, B., G. Fröhlich, and V. Lorenz (1991). "Quantitative experiments on phreatomagmatic explosions". *Journal of Volcanology and Geothermal Research* 48(3-4), pages 341–358. DOI: 10.1016/0377-0273(91)90050-a.